Synthesis and Characterization of Macrocycles *via* Migration Insertion Polymerization (MIP)

by

Ping Hsun Lo

A thesis

presented to the University of Waterloo

in fulfillment of the

thesis requirement for the degree of

Master of Science

in

Chemistry

Waterloo, Ontario, Canada, 2021

Author's Declaration

I hereby declare that I am the sole author of this thesis. This is a true copy of the thesis, including any required final revisions, as accepted by my examiners. I understand that my thesis may be made electronically available to the public.

Abstract

Migration insertion polymerization (MIP) of organometallic monomers, $^{P}FpC_X$ [^{P}Fp = $(PPh_2(CH_2)_3Cp)Fe(CO)_2$, C_X = $(CH_2)_{X-1}CH_3$, X = 12 or 18] were performed ether in bulk or solution. This MIP exclusively produced ring molecules including macrocycles and small rings. The small rings can be completely removed *via* precipitating the crude products in a poor solvent for the macrocycles. The cold ethanol and cold methanol were used as poor solvents to remove the small ring produced from the MIP of $^{P}FpC_{12}$ and $^{P}FpC_{18}$, respectively. The resultant macrocycles were characterized by using NMR, DLS, and TEM. The kinetic study indicated that the early stage of MIP included the oligomerization generating oligomers and the undesired monomer cyclization producing small rings. The resulting oligomers subsequently underwent cyclization, which generates macrocycles. The MIP under certain conditions such as lower temperature or bulk MIP of $^{P}FpC_{18}$, which favored oligomerization and suppressed monomer cyclization at the early stage, produced a relatively larger yield of $P(^{P}FpC_X)_n$ macrocycles. Both macrocycles are insoluble in DMF, methanol, and water, but are soluble in THF and toluene. Hexane is a poor solvent for $P(^{P}FpC_{12})_n$ but is a good solvent for $P(^{P}FpC_{18})_n$ due to the longer chain of C_{18}. The self-assembly of $P(^{P}FpC_X)_n$ were briefly studied. Both macrocycles can form stable colloids in DMSO/THF mixed solvents.

Acknowledgement

I would first like to express my deepest gratitude to my supervisor, Dr. Xiaosong Wang, for providing me this research opportunity as a Master student in his research group. He has encouraged me to be confident in myself and gave me chances to develop logical thinking and synthetic laboratory skills. His guidance and mentorship in the past two years are extremely important to me not just on the research but also in the future career.

I would also like to sincerely thank my committee member, Dr. Jean Duhamel and Dr. Juewen Liu, for providing valuable advice and suggestions on my research work.

I would like to thank Janet Venne and Mishi Groh for their technical supports on NMR and TEM instrumentations. I would also like to thank Catherine Van Esch for her generous help during my master's studies at the University of Waterloo to ensure that I can finish all graduation requirements and graduate on time.

I would also like to thank all my wonderful lab mates and friends, including Audren Luis Marquez, Snehasish Mondal, Anni Pan, I-Hsuan Yeh, Yang Yang, and Aaron Leung for always being supportive and there for me.

Last but not least, I would like to give my biggest appreciation to my parents and siblings for all their unparalleled love and understanding. Their patience, support, and unceasing encouragement were crucial in my milestone of master's program.

Thank you to everyone I have met in this amazing journey!

Dedication

I would like to dedicate my work to my parents and siblings, who have given me their unconditional love and unceasing encouragement since the beginning.

Table of Contents

List of Figures

List of Schemes

List of Tables

List of Abbreviations

AFM	Atomic force microscope
^{Cl}FpR	$(Cl(CH_2)_3Cp)Fe(CO)_2R$
Cp	Cyclopentadienyl
c-PFS	Cyclic poly(ferrocenylsilane)
DCM	Dichloromethane
DMF	Dimethylformamide
DMSO	Dimethylsulfoxide
DLS	Dynamic light scattering
DP	Degree of polymerization
Fp	$CpFe(CO)_2$
Fp_2	Cyclopentadienyl dicarbonyl iron dimer
FpK	Cyclopentadienyl dicarbonyl iron potassium
FpC_3P	$CpFe(CO)_2[(CH_2)_3PPh_2]]$
FpC_6P	$CpFe(CO)_2[(CH_2)_6PPh_2]]$
FpR	$CpFe(CO)_2R$
GPC	Gel permeation chromatography
IR	Infrared spectroscopy
MC	Metal-carbonyl
MIC	Migratory insertion cyclization
MIP	Migration insertion polymerization
MIR	Migratory insertion reaction

MW	Molecular weight
NMR	Nuclear magnetic resonance
PDI	Polydispersity index
$P(FpC_3P)_n$	Poly(cyclopentadienyl carbonyl diphenylphosphinopropyl iron)
$P(FpC_6P)_n$	Poly(cyclopentadienyl carbonyl diphenylphosphinohexyl iron)
^{P}Fp	$(PPh_2(CH_2)_3Cp)Fe(CO)_2$
^{P}FpR	$(PPh_2(CH_2)_3Cp)Fe(CO)_2R$
$P(^{P}FpC_6)_n$	$Poly[(PPh_2(CH_2)_3Cp)Fe(CO)_2(CH_2)_6]$
$P(^{P}FpC_{12})_n$	$Poly[(PPh_2(CH_2)_3Cp)Fe(CO)_2(CH_2)_{12}]$
$P(^{P}FpC_{18})_n$	$Poly[(PPh_2(CH_2)_3Cp)Fe(CO)_2(CH_2)_{18}]$
PFS	Polyferrocenylsilane
PS	Polystyrene
RB	Round bottom
ROP	Ring-opening polymerization
TEM	Transmission electron microscope
THF	Tetrahydrofuran

1.0 Introduction

The design and synthesis of polymers (or macromolecules) with various architectures is a fundamental research topic. For example, the synthesis and characterization of cyclic polymers have been the subject of ongoing research for decades.[1,2] Cyclic polymers, which do not have end-groups in comparison with linear polymers, exhibit different chemical and physical properties from their linear counterparts. A substantial amount of research has indicated that macrocycles possess unique properties, including higher glass transition temperature (T_g), lower intrinsic viscosity, smaller hydrodynamic volume, and radius of gyration (R_g).[1-3] Application of macrocycles in the field of self-assembly field has received increasing interest in recent years.[4,5]

1.1 Synthetic routes for macromolecules

There are two major traditional techniques for synthesizing cyclic polymers: ring-closure and ring-expansion. Ring-closure polymerization involves the synthesis of linear precursors with controlled molecular weight (MW) *via* oligomerization, followed by coupling reactions of the functional end-groups *via* intramolecular cyclization. Ring-closure reaction is an effective and powerful method for synthesizing macromolecules because it is applicable to a wide variety of molecules. However, some inherent deficiencies remain. For instance, a high dilution is often required to favor the intramolecular ring-closure process. This can significantly influence the purity and yield of macromolecules as intermolecular reactions still occur which require the separation of the macrocycles rand by-products formed intra- and intermolecularly, respectively. [6-8]

For example, Kubo *et al.* reported the ring-closing polymerization of cyclic polystyrene (PS), as shown in Scheme 1.1.[9] A linear PS chain with a carboxyl and an amino end group was first prepared as precursor. This was then followed by an intramolecular coupling cyclization

between the end groups under a highly diluted condition, resulting in a cyclic PS with a MW of *ca.* 2000 g/mol.[9]

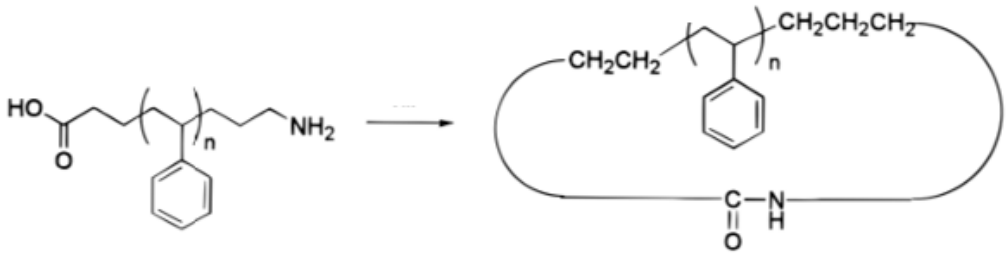

Scheme 1.1. Synthesis of cyclic PS *via* ring-closing process.[9]

Ring-expansion polymerization can be initiated by the insertion of a monomer into an activated cyclic chain. The propagation of the chain is achieved by analogous insertion of additional monomers. This method is effective because of the absence of linear intermediates, which produces cyclic polymers in a high yield with a broad range of MW. However, due to the restriction of the cyclic initiator, a limited number of systems can be synthesized by this method.[6,10]

For example, Kricheldorf *et al.* reported the synthesis of a cyclic polyester using cyclic tin initiator, 2,2-dibutyl-1,3-dioxa-2-stannane, at 75 °C as shown in Scheme 1.2.[11] During the polymerization, the cyclic monomer, beta-butyrolactone, is inserted into the initiator, 2,2-dibutyl-1,3-dioxa-2-stannanes, forming cyclic polyester.

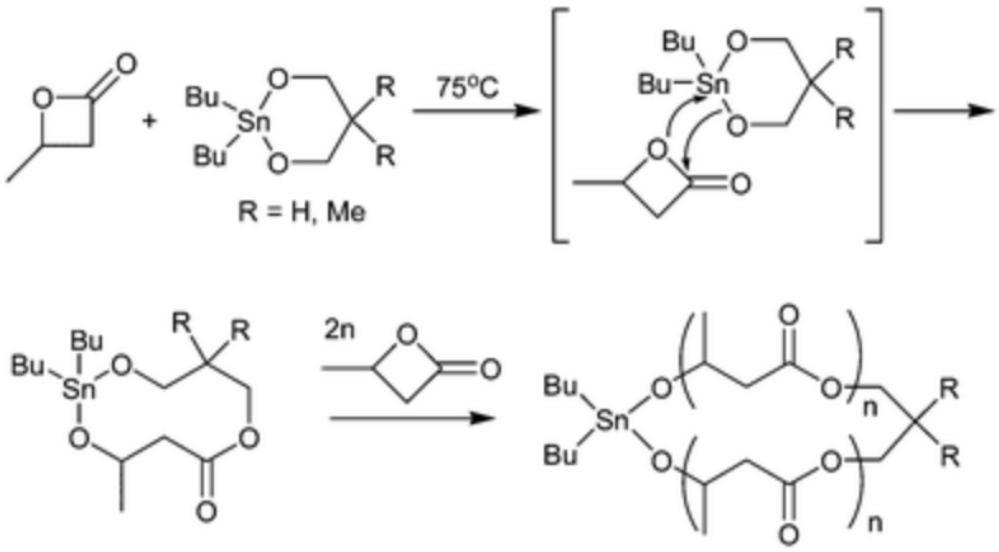

Scheme 1.2. Synthesis of cyclic polyester *via* ring-expansion polymerization.[11]

1.2 Metal-containing cyclic polymers

The introduction of metal-containing complexes into polymers has provided new opportunities for the synthesis of cyclic polymers with unique properties. Macrocycles have been prepared but some difficulties remain to synthesize pure and high molecular weight cyclic polymers. Manners *et al.* synthesized cyclic polyferrocenylsilane (c-PFS) in high yields and high MW *via* photocontrolled ring-opening polymerization (ROP) initiated by a neutral Lewis donor, 4,4'-dimethyl-2,2'-bipyridine (Me_2bpy) (Scheme 1.3).[12] The ROP generates linear macromolecules with Cp anions as active species, which tends to backbite the other chain end in the same macromolecules to close the polymer ring. This backbiting process was promoted by the Cp anions acting as a stronger ligand to replace the Me_2bpy that weakly interacted with the soft Fe^{II} center. The ROP of PFS produces several products such as unreacted monomer, linear polymer, cyclic oligomers ($x < 8$), and cyclic polymers ($x \geq 8$). The fraction of these products was influenced by the experimental conditions such as concentration, temperature, and irradiation time.

When higher concentration, longer irradiation time, and lower temperature were used, high MW c-PFS were favored.[12]

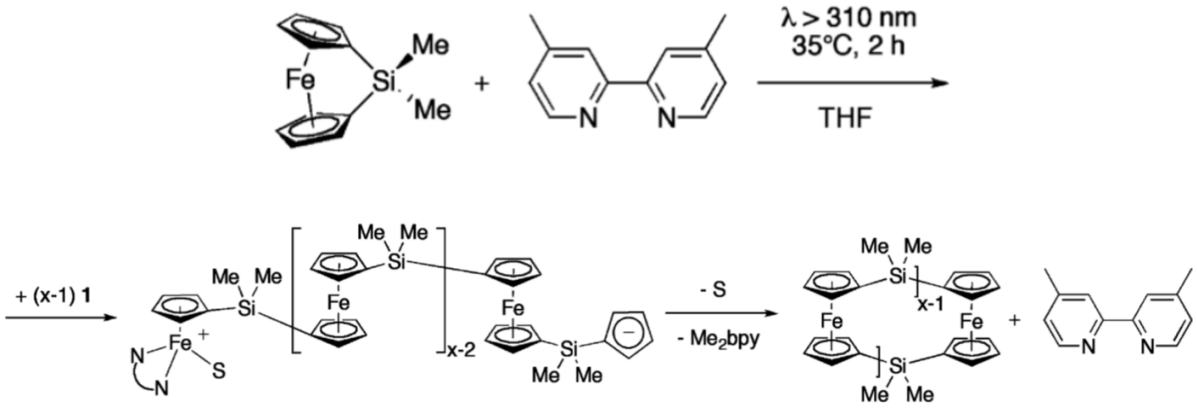

Scheme 1.3. Polymerization of PFS *via* backbiting reaction.[12]

1.3 Migration Insertion Polymerization

Migratory insertion reaction (MIR)[13-15] is a fundamental organometallic reaction. During this reaction, the combination of two adjacent ligands forms a new ligand, which decreases the overall electron count of the organometallic complex by two and forms an empty orbital on the central metal atom as shown in Scheme 1.4. Therefore, the empty orbital can take an upcoming ligand forming a new coordination bond with the metal.

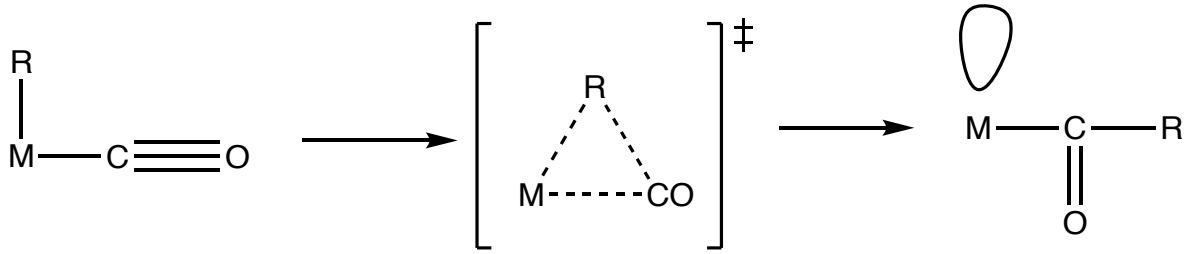

Scheme 1.4. MIR *via* CO insertion.[16]

Wang *et al.* previously developed migration insertion polymerization (MIP) by following the MIR mechanism.[18] They reported the synthesis of a bifunctional A-B type monomer that can

undergo polymerization *via* MIR and step-growth processes. The monomer, cyclopentadienyl dicarbonyldiphenylphosphinopropyl iron (FpC_3P), contains an iron complex (Fp) capable of migratory insertion reaction and a neutral phosphine ligand applicable of intermolecular coordination for a step-growth polymerization. FpC_3P, with the Fp group tethered with the phosphine ligand *via* a propyl spacer, was synthesized by a salt elimination reaction of cyclopentadienyl dicarbonyl iron potassium (FpK) with 1-chloropropyldiphenylphosphide (Scheme 1.5). The MIP of FpC_3P is initiated at an elevated temperature without any initiator (Scheme 1.6). As a result, an acyl ligand is formed from the combination of CO and alkyl ligands and an incoming phosphine ligand can coordinate through the empty orbital on iron. The MIP of FpC_3P generates air stable macromolecules, $P(FpC_3P)_n$, with narrow molecular weight distribution.[18] $P(FpC_3P)_n$ is soluble in numerous organic solvents such as THF, DMSO, and DCM, but is insoluble in water; and has a highest M_n of about 12,000 g/mol and a PDI of 1.28.[18] The development of MIP opens new possibilities for synthesizing metal-containing polymers.

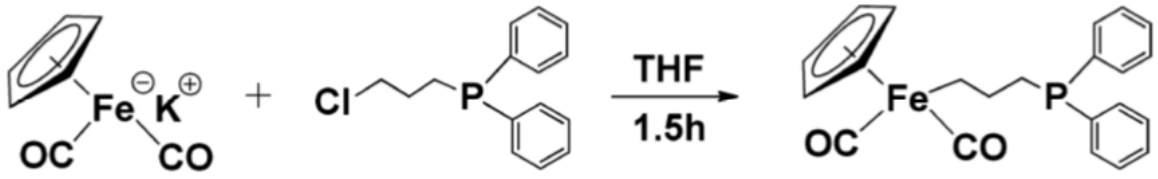

Scheme 1.5. Synthesis of FpC_3P.[18]

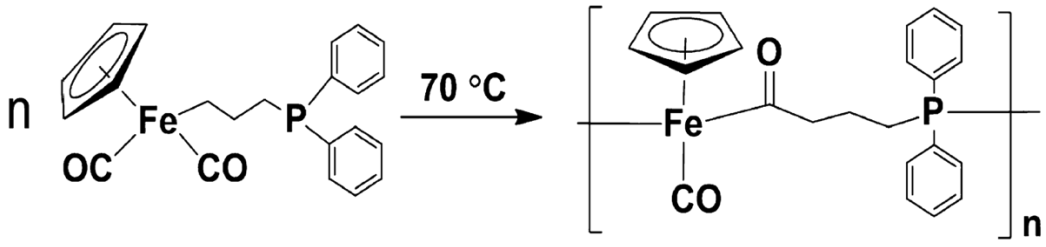

Scheme 1.6. MIP of FpC_3P.[18]

The polymerization of FpC_3P was concentration- and temperature-dependent (Figure 1.1).[19] FpC_3P underwent either intra- or intermolecular reactions in solution. Table 1.1 shows the resulting products from the reactions of FpC_3P under various conditions. As shown in Table 1.1 (entries 1 and 2), when the reaction was performed at room temperature with low FpC_3P concentration (1% by weight), five-membered rings were the major products in a yield of over 90%. Fp derivatives can release CO ligand and MIR requires a relatively higher temperature.[20,21] Consequently, intramolecular cyclization of FpC_3P *via* CO release was the major reactions. When the reaction temperature was increased to 40 and 70 °C (Table 1.1 entries 3 and 4) with low solution concentration, more six-membered cyclic Fp acyl derivatives and $P(FpC_3P)_n$ were formed. MIR was promoted at higher temperature, as a result, more products were produced from either intra- or intermolecular MIR. When the reaction temperature was kept at 70 °C and the solution concentration was increased (entries 5-7), the resulting intermolecular products increased significantly. Therefore, a high monomer concentration and a high reaction temperature are required for MIP of FpC_3P.[19]

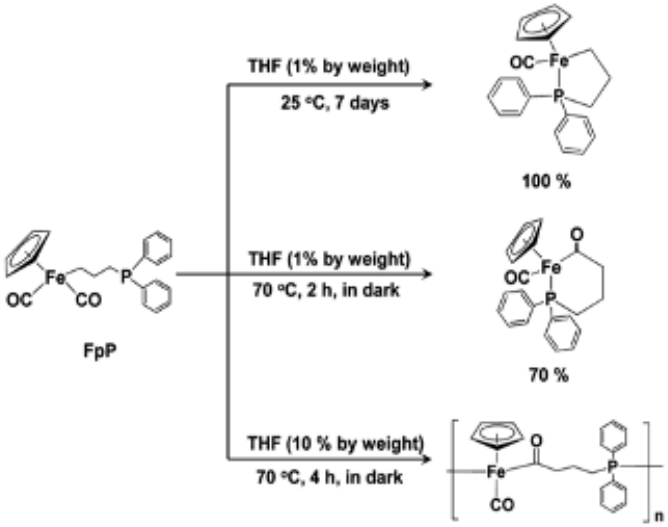

Figure 1.1. The effect of concentration and temperature on the reactions of FpC_3P in THF.[19]

Table 1.1. The effect of concentration and temperature on the reactions of FpC_3P in THF or hexane.[19]

					rel conversion (%)[a]		
entry	solvent	temp (°C)	concentration (wt %)	time	1	2	3
1	hexane	25	1.0	7 days	93.5	2.8	3.7
2	THF	25	1.0	7 days	99.8	0.1	0.08
3	THF	40	1.0	6 h	76.0	12.8	11.2
4	THF	70	1.0	4 h	51.8	36.8	11.40
5	THF	70	2.0	4 h	13	40.7	46.3
6	THF	70	5.0	4 h	8.6	21	70.4
7	THF	70	10	4 h	5.0	5.4	89.6

[a] **1** and **2** represent intramolecular cyclic complexes, while **3** represents intermolecular MIP products, as shown in Scheme 1.

FpC_6P, with C_6 to replace C_3, was synthesized for the MIP to generate $P(FpC_6P)_n$ (Scheme 1.7). Figure 1.2 illustrates the ^{31}P NMR spectra for the crude products of $P(FpC_6P)_n$ and $P(FpC_3P)_n$ resulting from bulk MIP at 70°C. As shown in Figure 1.2 (a), only two peaks are observed; one at 74 ppm which is due to the coordinated phosphorus and another peak at 30 ppm which can be assigned to the oxidized phosphine end group. The ^{31}P NMR spectra of $P(FpC_3P)_n$ crude products (Figure 1.2 (b)) shows two additional peaks at 109 and 68 ppm which are attributed to the phosphorous in five-membered and six-membered rings,[19] suggesting that some monomers underwent intramolecular cyclization. Hence, longer alkyl chain between Fp and phosphine can render intramolecular cyclization reactions unfavourable in bulk polymerization.

The effect of polymerization conditions on MIP of FpC_6P were also studied. When the FpC_6P monomers were heated at 60 °C for 14 hours, oligomers with a DP of 3 were obtained. The molecular weights of $P(FpC_6P)_n$ were relatively increased when increasing the polymerization temperature to 90 °C and extending the polymerization time to 48 hours. However, the DP for the $P(FpC_6P)_n$ was limited to 24, even when the temperature was heated to 130 °C. This can be attributed to the decreased reactivity of the end groups due to steric effect during MIP.[25]

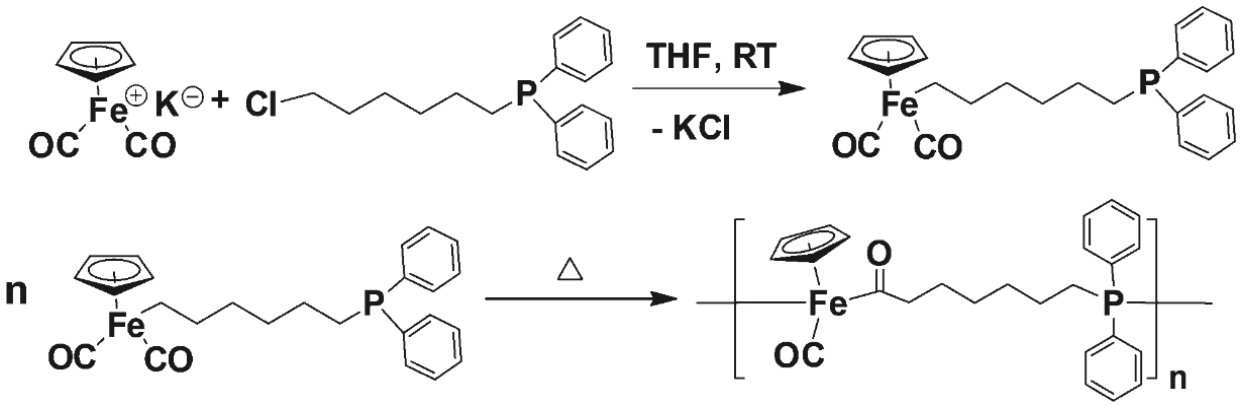

Scheme 1.7. Synthesis of FpC_6P and MIP of FpC_6P.[25]

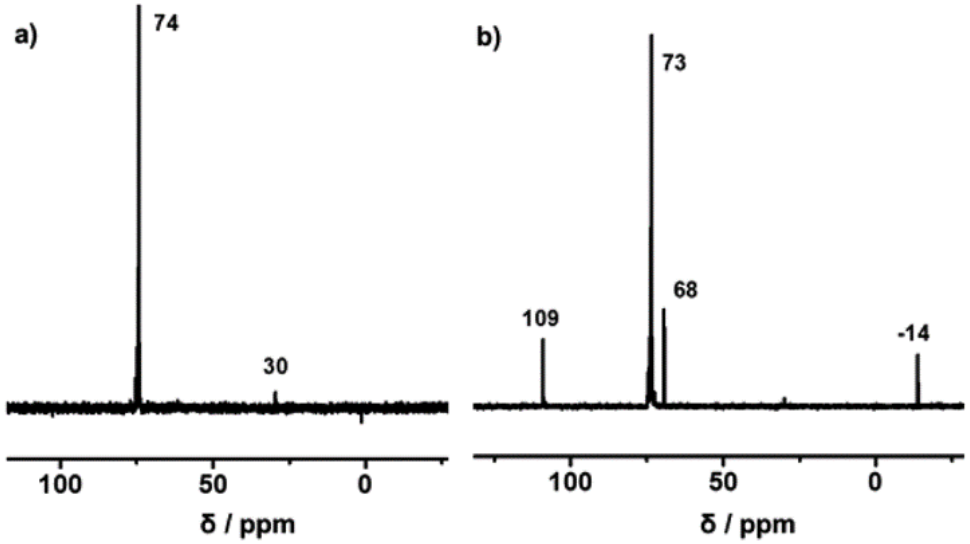

Figure 1.2. ^{31}P NMR spectra for (a) $P(FpC_6P)_n$ and (b) $P(FpC_3P)_n$ crude products obtained from bulk MIP at 70 °C.[25]

Cp metal acyl complexes are generally thermally stable up till 110 to 120 °C.[22-24] When incorporating the complexes into polymer chains *via* MIP, thermal stability was enhanced. $P(FpC_3P)_n$ and $P(FpC_6P)_n$ are thermally stable up to 180 and 170 °C, respectively.[18,25] $P(FpC_6P)_n$ is soluble in numerous solvents such as THF, DCM, and toluene, but insoluble in hexane, methanol, and acetonitrile. The stability of $P(FpC_6P)_n$ in solvents were examined by comparing the

color of the solutions after aging. No obvious color change in THF was observed while the solution turned to brown in other good solvents such as DCM and toluene. The stability of $P(FpC_6P)_n$ in THF and DCM were further verified by time-dependent ^{31}P NMR as the main chain coordinated phosphorus remained in THF while only the oxidized phosphorus was observed in DCM systems, suggesting a better stability in THF. $P(FpC_6P)_n$ is stable in THF for three days. However, the polymer became less stable in the presence of H_2O_2 and began to decompose in three hours. When $P(FpC_6P)_n$ was exposed to LED light (wavelength: 400-410 nm), the degradation accelerated even more and was completed in 20 minutes because metal acyl complexes are light sensitive.[26]

The MIP of FpC_XP as AB-type monomers generates $P(FpC_XP)_n$ containing P-Fe coordination bonds in the same coordination direction. Ditopic Fp derivatives, FpC_xFp (1) (C_X = alkyl spacers, X = 3 or 6) and bi-functional phosphine, $PR_2C_YPR_2$ (2) (R = phenyl or isopropyl, C_Y = alkyl spacers, Y = 3 or 6) were designed as A-A, B-B types monomers for MIP.[27] The polymerization was carried out at elevated temperature. The resultant $P(1/2)_n$ is soluble in various organic solvents such as THF, CH_2Cl, and toluene, and is stable for more than 10 days in non-chlorinated solvents such as THF, suggesting a better stability than $P(FpC_xP)_n$. The stability of P(1/2) was further analyzed by TGA. The decomposition temperature (T_{dec}) for P(1/2) is in the range of 160-190 °C which is 40-70 °C higher than Fp acyl complexes.[23-24] Each pair of macromolecules, $P(1a/2a)_n$/$P(FpC_3P)_n$ and $P(1b/2b)_n$/$P(FpC_6P)_n$, has the same chemical composition, but with different direction of P-Fe coordination along the backbone. The glass transition temperature, T_g, for $P(1a/2a)_n$ and $P(1b/2b)_n$ are 133 and 98 °C,[24] respectively. The corresponding $P(FpC_XP)_n$ (X = 3, 6) has a T_g of 99 °C ($P(FpC_3P)_n$)[18] and 68 °C ($P(FpC_6P)_n$),[25] respectively. The higher T_g in $P(1/2)_n$ suggests that the opposite direction of P-Fe bonds along the backbone renders the macromolecules more rigid. The T_{dec} for $P(1a/2a)_n$ and $P(1b/2b)_n$ are 187

and 182 °C,[27] respectively, which are relatively more stable than $P(FpC_3P)_n$ (180 °C)[18] and ($P(FpC_6P)_n$ (170°C).[25] The improved thermal stability can be attributed to the metal coordination direction in the backbone. $P(FpC_XP)$ with P-Fe bonds arranged in the same direction are fully extended into a linear helical conformation.[28] $P(1/2)_n$ with opposite directions of P-Fe bonds may adopt a non-linear conformation. The less ordered chain conformation may reduce the possibility for the metal coordination bonds to interact with the external media.[27]

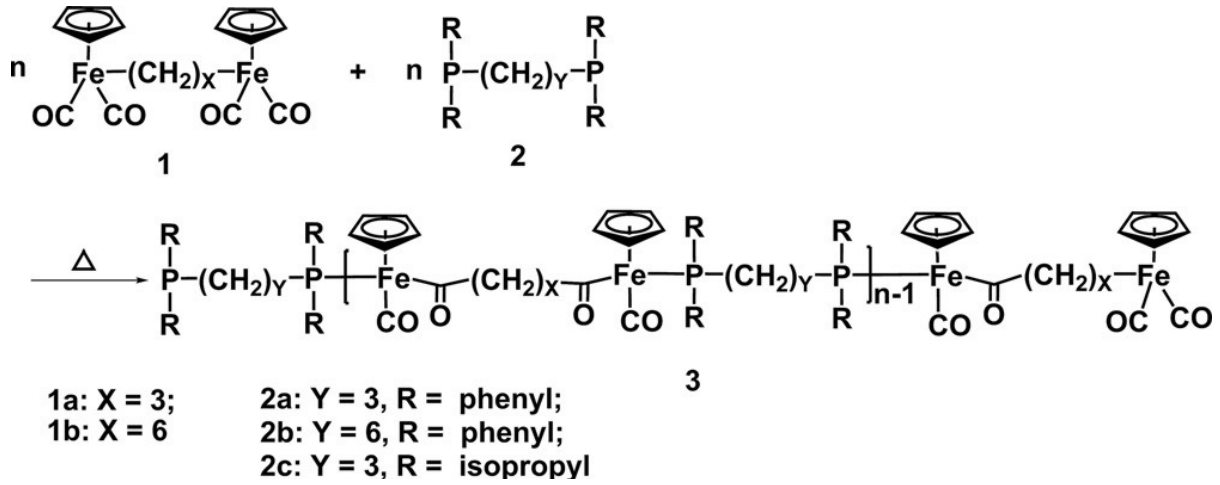

Scheme 1.8. MIP of ditopic Fp derivatives, FpC_xFp, and bi-functional phosphine, $PR_2C_YPR_2$.[27]

1.4 Migration Insertion Polymerization of ^{P}FpR

The backbone of $P(FpC_XP)_n$ (X = 3, 6) is constructed with phosphine coordinated iron-acyl units connected by alkyl spacers. The bond angle for the P-Fe-C repeating units is *ca.* 90°.[28] The piano-stool metal coordination geometry suggests that $P(FpC_XP)_n$ may adopt a cyclic conformation. MIP of FpC_6P in tetrahydrofuran (THF) produced linear $P(FpC_6P)_n$, while cyclic $P(FpC_6P)_n$ is produced when the THF/hexane mixed solvent is used. THF is a good solvent, in which the $P(FpC_6P)_n$ chain is fully extended. Hexane, on the other hand, is a poor solvent which causes chain contraction and favors the formation of cyclic structure.[28] ^{1}H and ^{31}P NMR

spectroscopies were used for characterization of $P(FpC_6P)_n$. Figure 1.3 illustrates the ^{31}P NMR spectra obtained from $P(FpC_6P)_n$ produced from THF (Figure 1.3 (a)) and a THF/hexane mixture (Figure 1.3 (b)). As shown in the Figure 1.3 (a), the spectrum for the linear $P(FpC_6P)_n$ shows two signals at 74 ppm (P1) and 35 ppm (P2), representing the phosphorus coordinated to Fe and the oxidized phosphine end groups, respectively. For the cyclic $P(FpC_6P)_n$ produced in THF/hexane solution, there is only one signal (P3) representing the iron-coordinated phosphine (Figure 1.3 (b))[28,29], suggesting that the cyclic $P(FpC_6P)_n$ is produced. These experiments indicate that the MIP of Fp-based monomers is a technique useful for the synthesis of cyclic molecules.

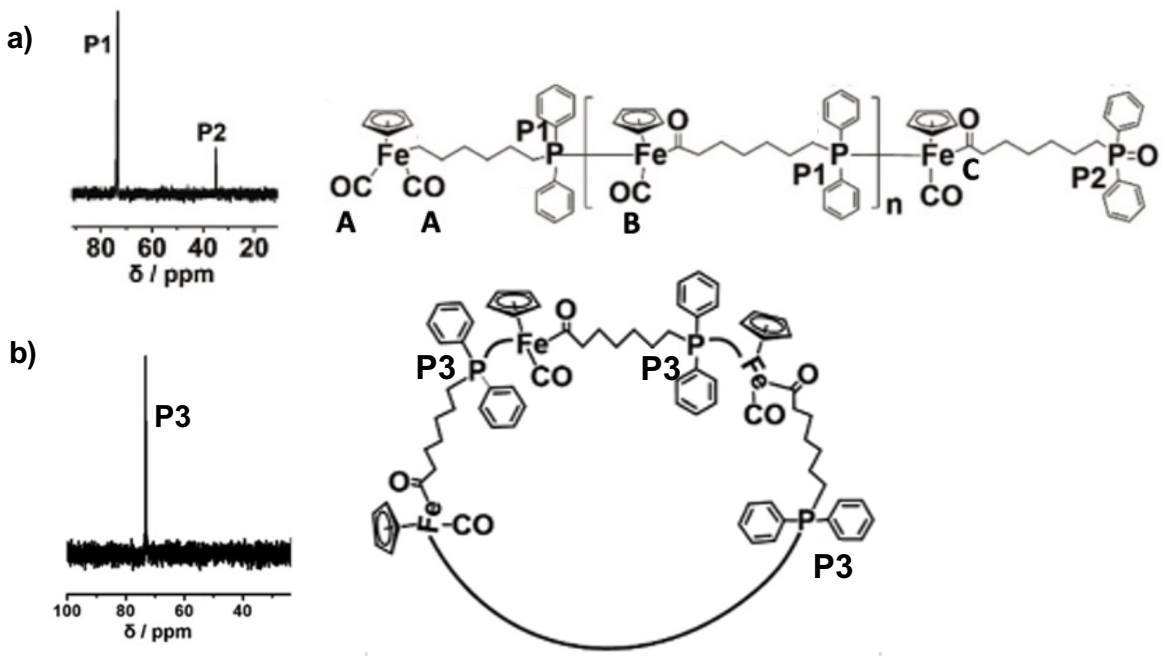

Figure 1.3. ^{31}P NMR spectra of $P(FpC_6P)_n$ produced in (a) THF and (b) THF/hexane mixture.[28]

The synthesized cyclic $P(FpC_6P)_n$ has a small molecular weight with n up to 6. As the cyclization is assisted by the contraction of the propagating chains in the mixed solvents containing a poor solvent, it is proposed to enhance the contraction by designing a monomer that can produce a flexible backbone. It is speculated that the Fp-based macromolecules would be flexible and easy

for the cyclization if Cp-Fe bonds with a low rotation energy were involved in the main chain.[27-28] With this idea, alkyl dicarbonyl diphenylphosphinopropylcyclopentadienyl iron (^{P}FpR, R = CH_3 or $(CH_2)_5CH_3$) was designed and synthesized as a MIP monomer (Scheme 1.9).[30] Simulations indicate that the macromolecules produced from this monomers have a short end-to-end distances, which favors for the targeted cyclization (Scheme 1.10). The MIP of ^{P}FpR in either bulk or THF without the poor solvent hexane was performed, and the crude products were precipitated in hexane to remove small molecules. The resulting macromolecules were analyzed by ^{1}H and ^{31}P NMR, transmission electron microscopy (TEM) and atomic force microscopy (AFM). Both ^{1}H and ^{31}P NMR analyses indicate that the resultant macromolecules do not contain end groups. The ^{31}P NMR spectrum only shows one chemical shift at 73.6 ppm due to the coordinated phosphorous atom in the main chain (Figure 1.4 (c)).[30] Figure 1.4 (a) displays the TEM image, which indicates a ring structure with bright centers. The bright center is caused by the rupture of the carbon film in the center of the rings after exposing the grid to the electron beam for a few minutes. The average diameter of the macrocycles is approximately 15 nm for the macrocycles of $P(^{P}FpC_6)_n$ produced in the bulk at 70 °C.[30] An AFM image of $P(^{P}FpR)_{n.}$ is displayed in Figure 1.4 (b), which indicates a donut-like morphology supporting the formation of macrocycles.

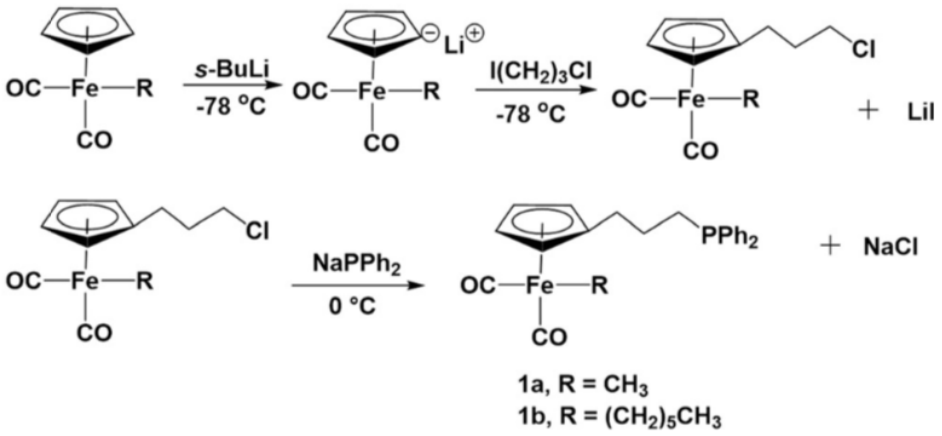

Scheme 1.9. Synthesis of ^{P}FpR.[30]

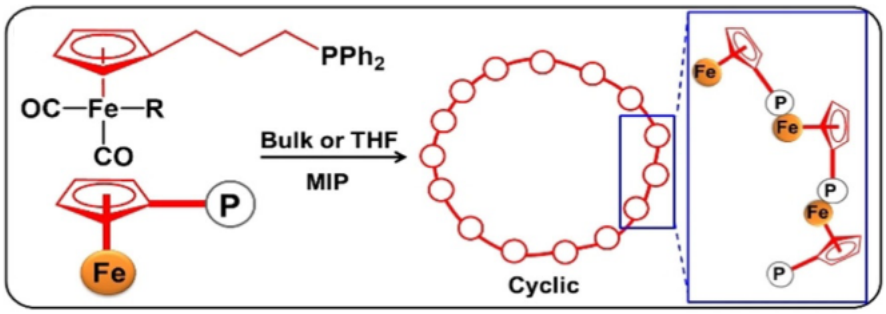

Scheme 1.10. MIP of ^{P}FpR.[30]

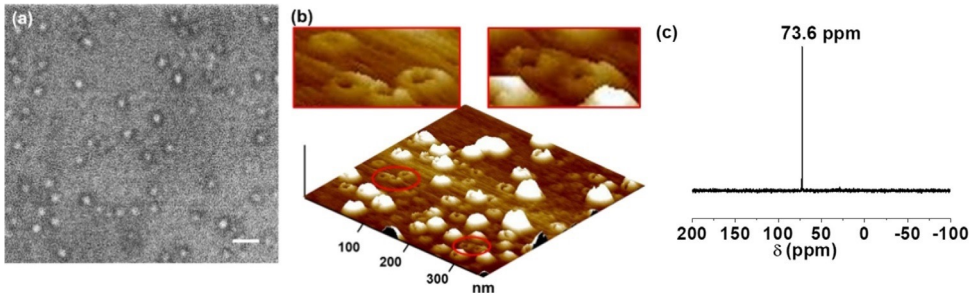

Figure 1.4. (a) TEM image, (b) AFM image, (c) ^{31}P NMR spectrum of P(^{P}FpR)$_n$. The macromolecules were purified by precipitation of the crude products in hexane.[30]

1.5 Competition between the formation of macrocycles of $P(^{P}FpC_6)_n$ and $^{P}FpC_6$ small rings

Migratory insertion polymerization of $^{P}FpC_6$ involved competitive cyclization between the MIP ring-closing polymerization and monomer cyclization, which generated $P(^{P}FpC_6)_n$ macrocycles and $^{P}FpC_6$ small rings (Figure 1.5).[31] Monomer cyclization occurred in the early stage of MIP while the growing polymer chains cyclized without producing linear analogues. The ^{31}P NMR spectrum of the crude products and the isolated components of the reaction mixture are shown in Figure 1.6. Two peaks at 72.3 and 71.5 ppm appears at 48 hours of polymerization representing the phosphorous in the macrocycles $P(^{P}FpC_6)_n$ and the $^{P}FpC_6$ small rings, respectively (Figure 1.6 (a)). $P(^{P}FpC_6)_n$ and $^{P}FpC_6$ small rings can be separated by adding the THF solution of the crude products to hexane, which only precipitates the macromolecules. The precipitates only show a single peak at 72.3 ppm due to the macrocycles, and the filtrate reveals one peak at 71.6 ppm due to the small rings (Figure 1.6 (b)).

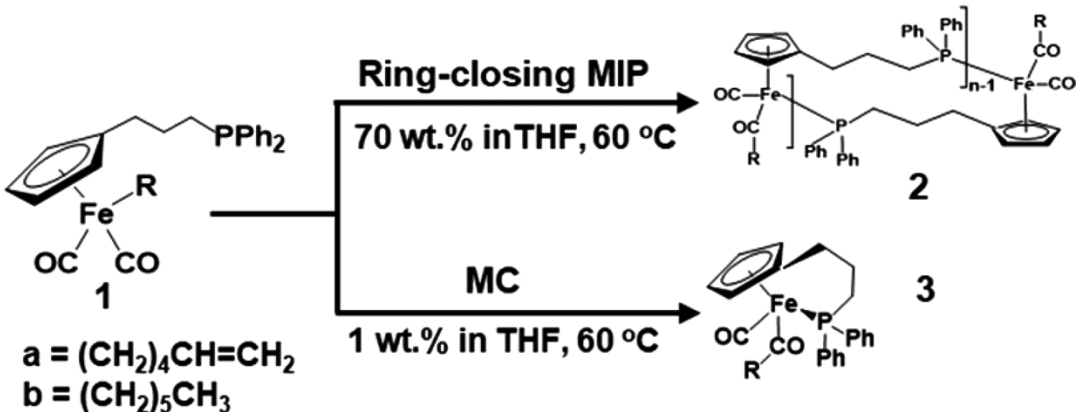

Figure 1.5. Reactions of $^{P}FpC_6$ in THF.[31]

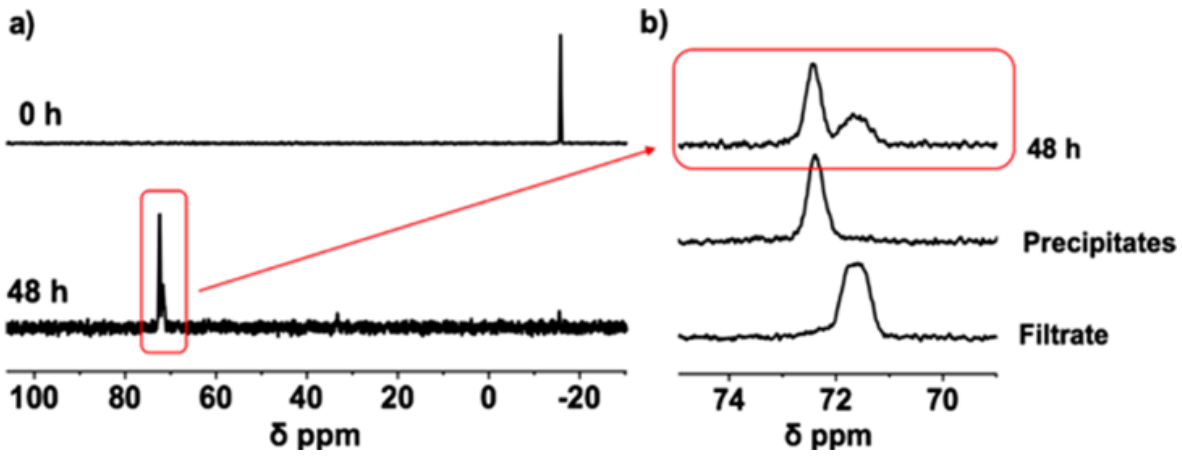

Figure 1.6. (a) ^{31}P NMR spectra of $^{P}FpC_6$ before and after MIP in bulk at 105 °C for 48 hours and (b) ^{31}P NMR spectra for $P(^{P}FpC_6)_n$ and $^{P}FpC_6$ small rings.[31]

The concentration effect of $^{P}FpC_6$ for the production of $P(^{P}FpC_6)_n$ and $^{P}FpC_6$ small rings was further investigated. Figure 1.7 displays the crude products prepared by MIP of $^{P}FpC_6$ at 60 °C for 48 hours. When the MIP of $^{P}FpC_6$ was performed with an extremely low concentration (1 wt %), only one signal at 71.5 ppm is observed, suggesting that the monomer cyclization is the only reaction that happens and that no ring-closing MIP occurs. Upon increasing the monomer concentration, the peak intensity at 71.5 ppm decreased, indicating that monomer cyclization is suppressed by a higher monomer concentration. This is probably due to the formation of small rings, which is favored at lower concentration.[32] Monomer cyclization is noticeably suppressed for the systems with concentration above 70 wt % as the signal at 71.5 ppm is weak and the majority of the products are $P(^{P}FpC_6)_n$. Intermolecular reaction is favored in higher concentration systems to grow polymer chain which reduces monomer cyclization. The growing chain eventually cyclized and formed macrocycles which is attributed to the nonlinear coordination geometry and Fe-Cp bonds in the backbone.[30,31]

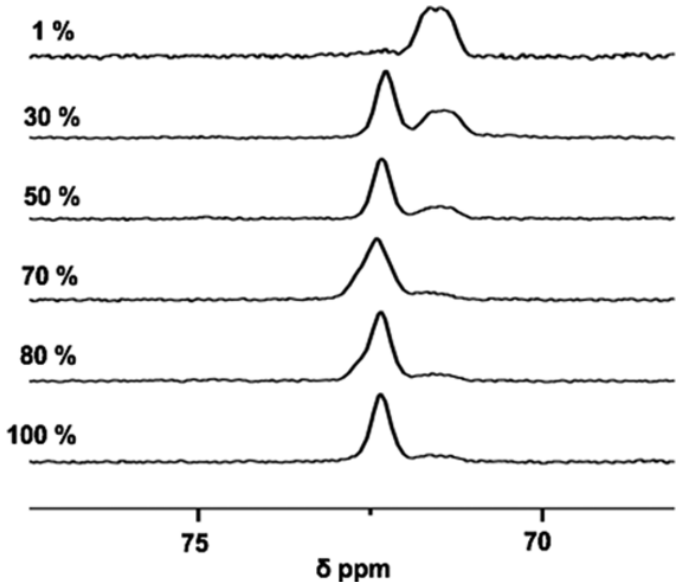

Figure 1.7. 31P NMR spectra of the crude product prepared by MIP of $^{P}FpC_6$ in THF with various monomer concentration at 60 °C for 48 hours.[31]

1.6 Self-assembly of $P(FpC_3P)_n$ and $P(^{P}FpR)_n$

$P(FpC_3P)_n$ linear macromolecules are able to self-assemble into uniform and stable colloids with a narrow size distribution in water[33], although $P(FpC_3P)_n$ is hydrophobic. One reason is attributed to the hydration of the macromolecules *via* water-carbonyl interactions. The acyl COs are highly polarized with stronger electronegative charges on the oxygen and able to exert a stronger water-carbonyl interaction (WCI) compared to those for organic carbonyl polymers.[34,35] The self-assembly produces colloids with various morphologies, including lamellae and vesicles, depending on the co-solvent used for the experiments.[33]

Fp-based macromolecules have a large dipole moment due to the presence of polar Fp groups, which increases with the degree of polymerization. This property appears to be important, and it has an effect on the solution behaviour and the MIP behaviour. MIP in THF for the synthesis of linear $P(FpC_3P)_n$ generates a small amount of THF-insoluble precipitates, which is possibly

caused by the enhanced dipole-dipole interactions with the growth of the chain.[19,37] The resultant THF-soluble macromolecules are short chains with a degree of polymerization of 9. However, the MIP for the synthesis of $P(^{P}FpC_6)_{28}$ cyclic macrocycles in THF produces no precipitates, and the degree of polymerization for the resultant macromolecules can be up to 46.

This behaviour is explained by the larger excluded volume of the macrocycles as indicated by larger R_g/R_h ratios (R_g: radius of gyration; R_h: hydrodynamic radius),[38,39] which can be attributed to the stiffness of the organometallic backbone.[30] Excluded volume (EV) is a type of repulsive force that prevents molecules in solution from approaching each other. Therefore, the balance between the EV and dipole-dipole interaction renders $P(^{P}FpC_6)_{28}$ soluble in THF. By the addition of hexane to enhance the attractive interactions, $P(^{P}FpC_6)_{28}$ macrocycles can self-assemble into nanotubes *via* a face-to-face stacking of the ring molecules.[40] Various amounts of hexane were added instantaneously to the THF solution of $P(^{P}FpC_6)_{28}$ macrocycles (1 mL, 1 mg/mL). Self-assembly occurs when the added hexane is more than 0.60 mL, and the resulting assemblies can be analyzed by TEM. Figure 1.8 shows the TEM images of $P(^{P}FpC_6)_{28}$ in THF solution without and with addition of hexane. As shown in Figure (1.8 (a)), individual macrocycles are observed in the image. When 0.75 mL of hexane was added instantaneously to the THF solution, the cyclic nanotubes are observed (Figure 1.8 (b)). The diameters of the assembled cyclic nanotubes are ranged from 0.5 to 1.8 μm. $P(^{P}FpC_6)_{28}$ macrocycles underwent self-assembly into cyclic nanotubes by overcoming the repulsion forces.

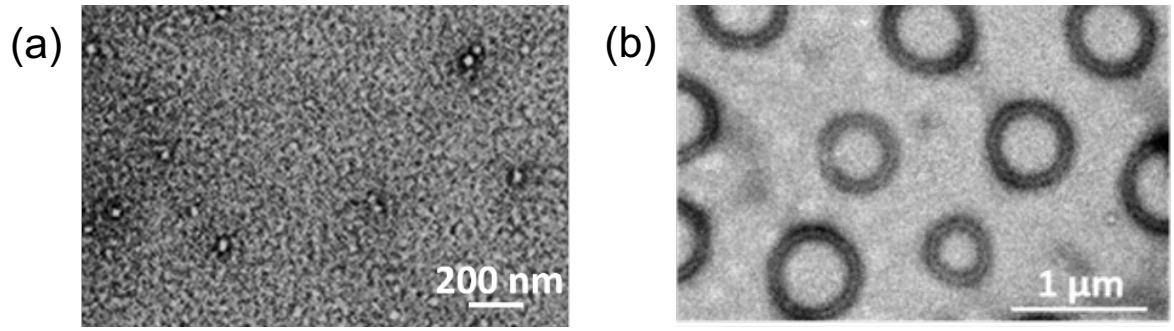

Figure 1.8. TEM images of (a) P(^{P}FpC$_6$)$_{28}$ in THF and (b) the assembly of P(^{P}FpR)$_{28}$ macrocycles by instantaneous addition of 0.75 ml into 1.0 mL of a THF solution of P(^{P}FpR)$_{28}$.[40]

Herein, ^{P}FpC$_X$ [^{P}Fp = (PPh$_2$(CH$_2$)$_3$Cp)Fe(CO)$_2$, CX = (CH$_2$)$_{X-1}$CH$_3$, X = 12, 18] with long alkyl chain were synthesized and the MIP of ^{P}FpC$_X$ were performed at various conditions. The goal of this project is to study the effect of polymerization conditions and the types of monomers on the MIP of ^{P}FpC$_X$, namely the competitive cyclization for the formation of small rings and macrocycles. The synthesized macrocycles are potentially useful for the investigation of self-assembly.

2.0 Experimental

Materials: All experiments were performed under an atmosphere of dry nitrogen. THF was freshly distilled from Na/benzophenone under nitrogen. Sodium (Na), benzophenone, 1-bromododecane, 1-chloro-3-iodopropane, sec-butyllithium solution (1.4 M in cyclohexane), and potassium (K) were purchased from Sigma-Aldrich. Cyclopentadienyliron dicarbonyl dimer (Fp_2) was purchased from Strem Chemicals Inc. Chlorodiphenylphosphine and 1-chlorooctadecane were purchased from Tokyo Chemical Industry (TCI). All chemicals were used as received unless otherwise indicated.

Instrumentation: ^{1}H and ^{31}P NMR spectra were obtained on a Bruker Avance 300 (300 MHz) spectrometer at ambient temperature using $CDCl_3$ as the solvent. TEM images were obtained with a Philips CM10 transmission electron microscope. Molecular weights and molecular weight distributions were characterized using GPC. The Viscotek VE 2001 GPC was equipped with PolyAnalytik SupeRes mixed bed columns and a TDA 305 triple detector array including refractive index, viscosity, and dual-angle light scattering detectors. THF was used as eluent at a flow rate of 1.0 mL/min and polystyrene standards were used. Dynamic light scattering (DLS) was carried out at 25 °C using Malevern Zetasizer Nano90.

2.1 Synthesis of cyclopentadienyl dicarbonyliron potassium (FpK)

Potassium benzophenone ketyl was prepared by stirring benzophenone (5.20 g, 28.6 mmol) and potassium (1.12 g, 28.6 mmol) in a Schlenk round bottom flask containing distilled THF (120 mL). The reaction scheme is shown in Scheme 2.1. The solution immediately turned dark blue. After stirring at room temperature (23°C) for 2 hours, cyclopentadienyldicarbonyl iron dimer (Fp_2) (5.56 g, 15.7 mmol) was added to the solution and stirred at 23 °C for 2 hours. The dark blue color

disappeared upon the addition of Fp_2 and the solution became brown after stirring at 23 ºC for 2 hours. The solution was used directly without purification for further reactions.

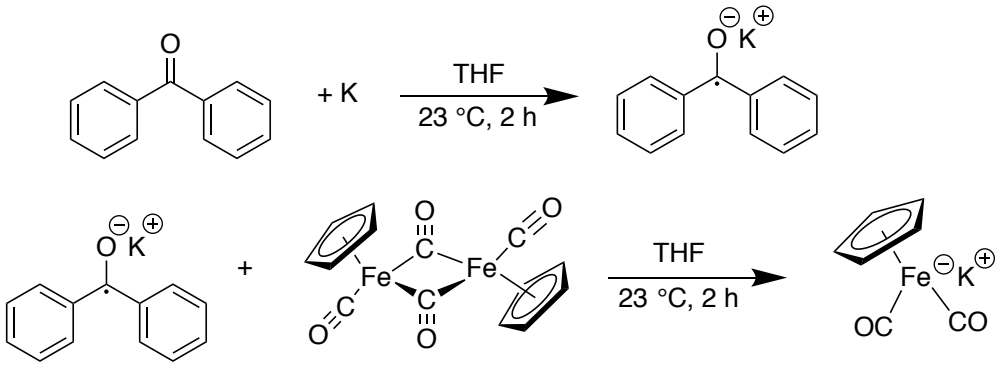

Scheme 2.1. Synthesis of FpK.

2.2 Synthesis of sodium diphenylphosphide (PPh_2Na, 0.5 M in THF)

PPh_2Na was prepared by stirring chlorodiphenylphosphine ($ClPPh_2$) (18.5 mL, 0.1 mol) and sodium (6.9g, 0.3 mol) in a Schlenk round bottom flask containing distilled THF (200 mL). The reaction scheme is shown in Scheme 2.2. The mixture was stirred at 40 °C for 3 days, resulting in a bright red solution. The solution was used directly without purification for further reactions.

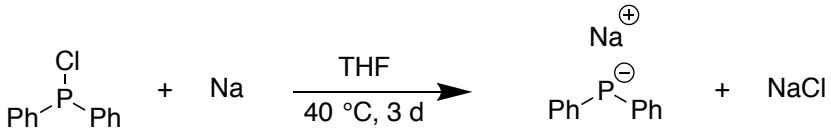

Scheme 2.2. Synthesis of $NaPPh_2$.

2.3 Synthesis of FpC_X (X = 12, 18)

The THF solution (120 mL) of FpK (6.17 g, 28.6 mmol) was cooled down to 0 °C by using an ice bath, and alkyl halide ($CH_3(CH_2)_{11}Br$ (6.41 g, 25.7 mmol) for FpC_{12} or $CH_3(CH_2)_{17}Cl$ (7.42 g, 25.7 mmol) for FpC_{18}) was added dropwise to the solution (Scheme 2.3). After addition, the ice

bath was removed, and the solution was warmed to room temperature. The reaction gradually turned brown to orange and was stirred at room temperature for 2 hours. Afterwards, THF was removed by using a rotatory evaporator resulting in a crude product, which was subsequently dissolved in a small amount of hexane. The hexane solution was passed through a Celite column to remove salts. The eluent was collected, and the hexane was removed by using a rotatory evaporator to yield the crude product. The crude product was further purified by a silica-gel column, using hexane as eluent. The orange band was collected, and the hexane was removed by using the rotatory evaporator, yielding an orange oil of both FpC_{12} and FpC_{18}. The FpC_{18} oil turned into a powder after being left at room temperature for 20 minutes. For FpC_{12}: Yield: 88 %. ^{1}H NMR ($CDCl_3$): 4.71 ppm (s, 5 H, $C_5\mathbf{H}_5$), 1.42 ppm (2 H, $FeC\mathbf{H}_2(CH_2)_{10}CH_3$), 1.26 ppm (10 H, $FeCH_2(C\mathbf{H}_2)_{10}CH_3$), 0.86 (H, $(CH_2)_{11}C\mathbf{H}_3$). For FpC_{18}: Yield: 85 %. ^{1}H NMR ($CDCl_3$): 4.70 ppm (s, 5 H, $C_5\mathbf{H}_5$), 1.43 ppm (2 H, $FeC\mathbf{H}_2(CH_2)_{16}CH_3$), 1.26 ppm (32 H, $FeCH_2(C\mathbf{H}_2)_{16}CH_3$), 0.86 (H, $(CH_2)_{11}C\mathbf{H}_3$).

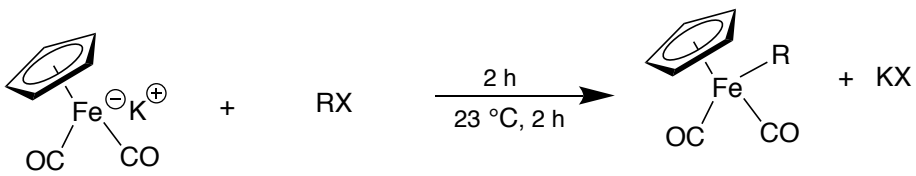

Scheme 2.3. Synthesis of FpC_x. For FpC_{12}, RX = $(CH_3(CH_2)_{11}Br$ and for FpC_{18}, RX = $CH_3(CH_2)_{17}Cl$.

2.4 Synthesis of $^{Cl}FpC_X$ (X = 12, 18)

FpC_X (FpC_{12}: 1.78 g, 5.15 mmol; FpC_{18}: 1.53 g, 3.55 mmol) was dissolved in THF (120 mL). The solution was cooled down to -78 °C by placing in a dry ice/acetone bath. *Sec*-butyllithium (1.4 M in cyclohexane; FpC_{12}: 5.52 mL, 7.72 mmol; FpC_{18}: 3.81 mL, 5.33 mmol)

was added to the solution dropwise and stirred at -78 °C for 30 minutes (Scheme 2.4). The solution gradually turned from yellow to dark red. Afterward, 1-chloro-3-iodopropane (FpC_{12}: 0.66 mL, 6.18 mmol; FpC_{18}: 0.46 mL, 4.27 mmol) was added dropwise at -78 °C. The ice bath was removed after the addition and the reaction was warmed to room temperature and stirred for 2 hours. The solution gradually turned from dark red to brown. THF was removed by using a rotatory evaporator resulting in a crude product, which was subsequently dissolved in a small amount of hexane. The hexane solution was then passed through a Celite column to remove salts. The eluent was collected, and the hexane was removed by using the rotatory evaporator. The resulting crude product was further purified by a silica-gel column using hexane (for $^{Cl}FpC_{12}$) or a mixture of hexane/DXM (10:1 v/v) (For $^{Cl}FpC_{18}$) as eluent. The first orange band was collected, and the solvent was removed by using a rotary evaporator, yielding an orange oil of unreacted FpC_X. Unreacted 1-chloro-3-iodopropnae eluted next and followed by another yellow band. The second yellow band was also collected, and the solvent was removed by using a rotatory evaporator to yield a yellow oil of $^{Cl}FpC_X$. For $^{Cl}FpC_{12}$: Yield: 45 %. ^{1}H NMR ($CDCl_3$): 4.59 ppm (s, 2 H, $C_5\mathbf{H}_4$), 4.55 ppm (s, 2 H, $C_5\mathbf{H}_4$), 3.55 ppm (t, 2 H, $C\mathbf{H}_2Cl$), 2.39 ppm (t, 2 h, $(C_5H_4)C\mathbf{H}_2$), 1.96 ppm (q, 2 H, $CH_2C\mathbf{H}_2CH_2Cl$), 1.42 ppm (2 H, $FeC\mathbf{H}_2(CH_2)_{10}CH_3$), 1.26 ppm (10 H, $FeCH_2(C\mathbf{H}_2)_{10}CH_3$), 0.86 (H, $(CH_2)_{11}C\mathbf{H}_3$). For $^{Cl}FpC_{18}$: Yield: 48 %. ^{1}H NMR ($CDCl_3$): 4.59 ppm (s, 2 H, $C_5\mathbf{H}_4$), 4.55 ppm (s, 2 H, $C_5\mathbf{H}_4$), 3.55 ppm (t, 2 H, $C\mathbf{H}_2Cl$), 2.40 ppm (t, 2 H, $(C_5H_4)C\mathbf{H}_2$), 1.96 ppm (q, 2 H, $CH_2C\mathbf{H}_2CH_2Cl$), 1.43 ppm (2 H, $FeC\mathbf{H}_2(CH_2)_{17}CH_3$), 1.26 ppm (10 H, $FeCH_2(C\mathbf{H}_2)_{17}CH_3$), 0.86 (H, $(CH_2)_{17}C\mathbf{H}_3$).

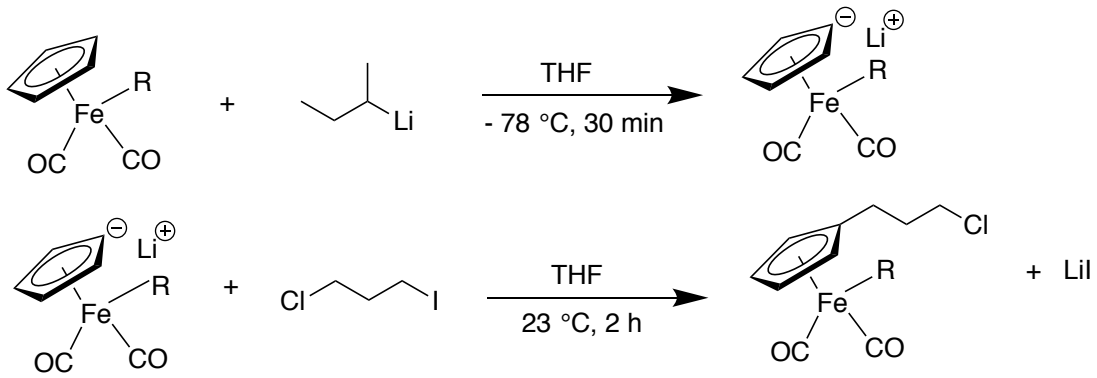

Scheme 2.4. Synthesis of FpC_x. For $^{Cl}FpC_{12}$: R = $(CH_3(CH_2)_{11}$ and for FpC_{18}: R = $CH_3(CH_2)_{17}$.

2.5 Synthesis of $^{P}FpC_X$ (X = 12, 18)

$^{Cl}FpC_X$ ($^{Cl}FpC_{12}$: 0.37 g, 0.87 mmol; $^{Cl}FpC_{18}$: 1.53 g, 3.55 mmol) was dissolved in THF (80 mL). The solution was cooled down to 0 °C by placing in an ice bath and $NaPPh_2$ solution (0.5 M in THF ($^{P}FpC_{12}$: 3.50 mL, 1.75 mmol; $^{P}FpC_{18}$: 1.53 g, 3.55 mmol) was added dropwise into the reaction (Scheme 2.5). The ice bath was removed, and the solution was warmed to room temperature and stirred for another 2 hours. The reaction turned from dark brown to orange. At the end of the reaction, degassed methanol (2 mL) was added to quench excess amount of $NaPPh_2$. THF was removed by using a rotatory evaporator, and the resulting crude product was dissolved in a small amount of hexane. The hexane solution was passed through a Celite column to remove NaCl. The eluent was collected, and hexane was removed by using a rotatory evaporator. The crude product was further purified by running a silica-gel column with a hexane/DCM (10:1 v/v) mixture as eluent. The yellow band was collected, and the solvents were removed, resulting in a yellow oil. For $^{P}FpC_{12}$: Yield: 47 %. ^{31}P NMR ($CDCl_3$): -15.7 ppm; ^{1}H NMR ($CDCl_3$): 7.58 – 7.31 ppm (m, 10 H, $P(C_6H_5)_2$), 4.55 ppm (s, 2 H, $C_5\mathbf{H}_4$), 4.47 ppm (s, 2 H, $C_5\mathbf{H}_4$), 2.33 ppm (t, 2 H, $C\mathbf{H}_2PPh_2$), 2.06 ppm (t, 2 h, $(C_5H_4)C\mathbf{H}_2$), 1.65 ppm (2 H, $CH_2C\mathbf{H}_2CH_2P$), 1.39 ppm (2 H,

FeC**H**$_2$(CH$_2$)$_{10}$CH$_3$), 1.26 ppm (10 H, FeCH$_2$(C**H**$_2$)$_{10}$CH$_3$), 0.86 (H, (CH$_2$)$_{11}$C**H**$_3$). For ^{P}FpC$_{18}$: Yield: 45 %. ^{31}P NMR (CDCl$_3$): -15.7 ppm; ^{1}H NMR (CDCl$_3$): 7.58 – 7.30 ppm (m, 10 H, P(C$_6$H$_5$)$_2$), 4.55 ppm (s, 2 H, C$_5$**H**$_4$), 4.47 ppm (s, 2 H, C$_5$**H**$_4$), 2.33 ppm (t, 2 H, C**H**$_2$PPh$_2$), 2.06 ppm (t, 2 H, (C$_5$H$_4$)C**H**$_2$), 1.65 ppm (, 2 H, CH$_2$C**H**$_2$CH$_2$P), 1.38 ppm (2 H, FeC**H**$_2$(CH$_2$)$_{17}$CH$_3$), 1.25 ppm (10 H, FeCH$_2$(C**H**$_2$)$_{17}$CH$_3$), 0.86 (H, (CH$_2$)$_{17}$C**H**$_3$).

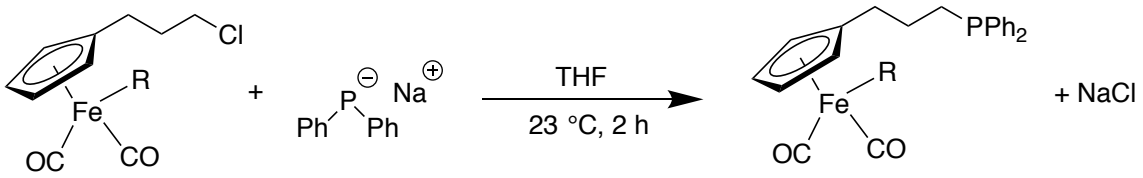

Scheme 2.5. Synthesis of ^{P}FpC$_X$. For ^{Cl}FpC$_{12}$: R = (CH$_3$(CH$_2$)$_{11}$ and for FpC$_{18}$: R = CH$_3$(CH$_2$)$_{17}$.

2.6 Synthesis of P(^{P}FpC$_X$)$_n$ macrocycles (X = 12, 18)

In a Schlenk flask containing ^{P}FpC$_X$ (^{P}FpC$_{12}$: 0.13 g, 0.23 mmol; ^{P}FpC$_{18}$: 0.28 g, 0.43 mmol), polymerization was initiated by heating the solution to 70 °C (Scheme 2.6). After 48 hours, the crude product was dissolved in 0.2 mL of THF and precipitated into 80 mL of cold ethanol (-50 °C, for P(^{P}FpC$_{12}$)$_n$) or methanol (-50 °C, for P(^{P}FpC$_{18}$)$_n$). P(^{P}FpC$_{12}$)$_n$ was separated by filtration and P(^{P}FpC$_{18}$)$_n$ was separated by centrifugation. The precipitates were dried under vacuum to yield yellow polymers. For P(^{P}FpC$_{12}$)$_n$: Yield: 75 %. ^{31}P NMR (CDCl$_3$): 72.5 ppm; ^{1}H NMR (CDCl$_3$): 7.37 – 7.23 ppm (br, 10 H, P(C$_6$**H**$_5$)$_2$), 4.08 – 3.95 ppm (m, 4 H, C$_5$**H**$_4$), 2.76 ppm (s, 1H, Fe(CO)C**H**$_2$(CH$_2$)$_8$CH$_3$), 2.52 ppm (s, 1 H, Fe(CO)C**H**$_2$(CH$_2$)$_8$CH$_3$), 2.25 – 2.12 ppm (m, 10 H, Fe(CO)C**H**$_2$(CH$_2$)$_8$CH$_3$), 1.25 ppm (2 H, CH$_2$C**H**$_2$CH$_2$P), 1.05 ppm (20 H, Fe(CO)CH$_2$(C**H**$_2$)$_8$CH$_3$), 0.83 ppm (s, 3H, Fe(CO)CH$_2$(CH$_2$)$_8$C**H**$_3$). For P(^{P}FpC$_{18}$)$_n$: Yield: 80 %. ^{31}P NMR (CDCl$_3$): 72.5 ppm; ^{1}H NMR (CDCl$_3$): 7.38 – 7.23 ppm (br, 10 H, P(C$_6$**H**$_5$)$_2$), 4.08 –

3.95 ppm (m, 4 H, $C_5\mathbf{H}_4$), 2.75 ppm (s, 1H, $Fe(CO)C\mathbf{H}_2(CH_2)_{16}CH_3$), 2.52 ppm (s, 1 H, $Fe(CO)C\mathbf{H}_2(CH_2)_{16}CH_3$), 2.25 – 2.12 ppm (m, 10 H, $Fe(CO)C\mathbf{H}_2(CH_2)_{16}CH_3$), 1.25 ppm (2 H, $CH_2C\mathbf{H}_2CH_2P$), 1.05 ppm (20 H, $Fe(CO)CH_2(C\mathbf{H}_2)_{16}CH_3$), 0.83 ppm (s, 3H, $Fe(CO)CH_2(CH_2)_{16}C\mathbf{H}_3$).

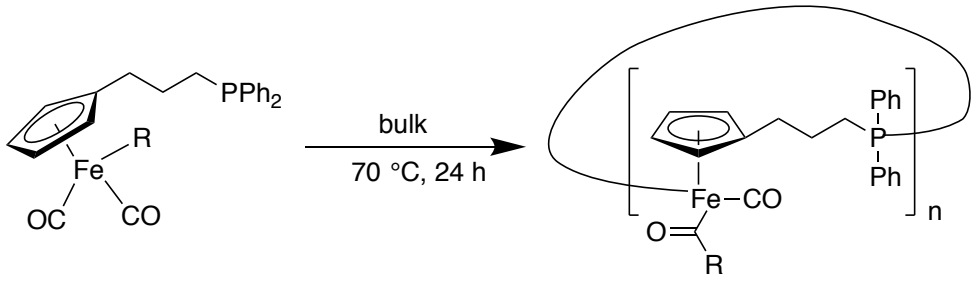

Scheme 2.6. Synthesis of $P(^PFpC_X)_n$. For $P(^PFpC_{12})_n$: R = $(CH_3(CH_2)_{11}$ and for $P(^PFpC_{18})_n$: R = $CH_3(CH_2)_{17}$.

2.7 Self-assembly of $P(^PFpC_X)_n$ (X = 12, 18) macrocycles

THF solutions of $P(^PFpC_X)_n$ (X = 12, 18) (1 mg/mL) were prepared first. 10 mL of poor solvents including hexane, DMSO, water, and methanol were added to the solution instantaneously resulting in a colloidal dispersion. The final concentration of $P(^PFpC_X)_n$ was 0.1 mg/mL. The colloidal dispersions were left at room temperature for a few days for aging experiments

3.0 Results and Discussion

3.1 Synthesis and characterization of $^{P}FpC_{12}$

$^{P}FpC_{12}$ was synthesized in three steps. First, FpC_{12} was synthesized *via* the reaction of Fp anion with 1-bromododecane at 23 °C in THF (Scheme 3.1). After the addition of 1-bromododecane, the solution turned from brown to orange. The THF was removed under vacuum after reacting for 2 hours, which yielded an orange oil. The crude product was purified by using Celite and silica gel columns. The purified product was characterized by ^{1}H NMR and the resultant spectrum is displayed in Figure 1. As shown in the figure, the signal at 4.7 ppm corresponds to the protons in the Cp ring.[42] The signal *a* at 1.42 ppm can be assigned to the protons in the CH_2 groups connected to the Fe atom and the signal *c* at 0.86 ppm can be assigned to the protons in the methyl group.[31] All of the other alkyl protons show a chemical shift at 1.26 ppm (*b* in Figure 3.1). The integration ratio of *c*/(*a*+*b*) is 3/22, matching the expected value for the designed FpC_{12}. This spectrum indicates that FpC_{12} was synthesized.

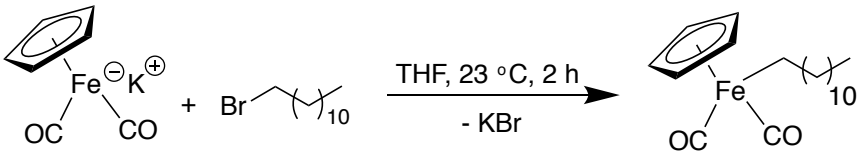

Scheme 3.1. Schematic illustration for the synthesis of FpC_{12}.

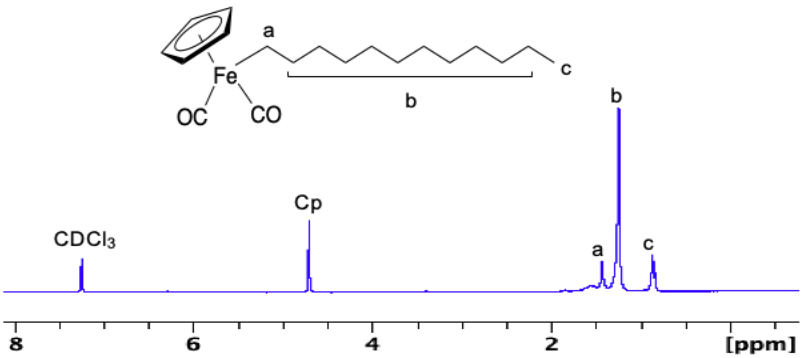

Figure 3.1. ^{1}H NMR ($CDCl_3$) spectra of FpC_{12}.

$^{Cl}FpC_{12}$ was then synthesized *via* the deprotonation of the Cp ring at -78 °C in THF by the addition of *sec*-butyllithium dropwise. The solution turned dark red, to which 1-chloro-3-iodopropnae was added. The reaction mixture was then warmed to 23 °C (Scheme 3.2) and the colour turned to green. The reaction gradually turned to brown after stirring at 23 °C for 2 hours. Afterwards, THF was removed under vacuum, which yielded a brown oil. The crude product was purified by using Celite and silica gel column. The purified product was characterized by ^{1}H NMR and the resultant spectrum is displayed in Figure 3.2. As shown in the figure, the signals at 4.59 ppm and 4.55 ppm correspond to the protons in the Cp ring.[30] Three signals, including *a* at 2.39 ppm, *b at* 1.96 ppm and *c* at 3.55 ppm, can be attributed to the protons in the propyl chloride chain.[30] Signal *d*, *e*, and *f* at 1.42, 1,26, and 0.86 ppm, respectively, can be assigned to the protons from the dodecyl chain.[30] The proton integration ratio of Cp/a/b/c/(d+e)/f is 4/2/2/2/22/3, matching the expected value for the designed $^{Cl}FpC_{12}$. This spectrum shows that $^{Cl}FpC_{12}$ was synthesized.

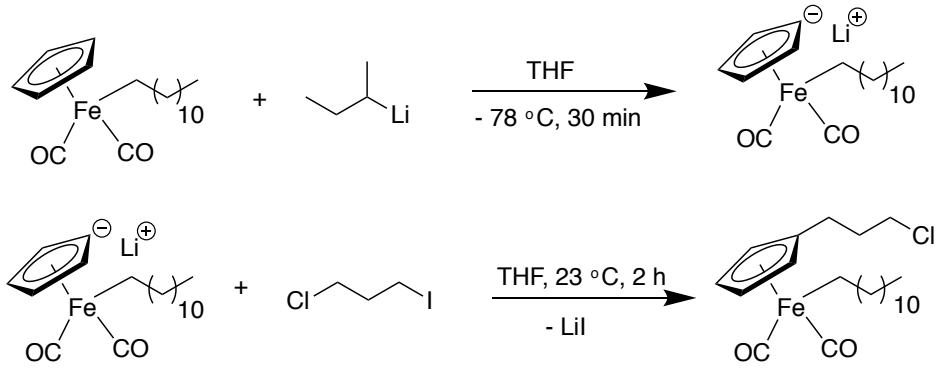

Scheme 3.2. Schematic illustration for the synthesis of $^{Cl}FpC_{12}$.

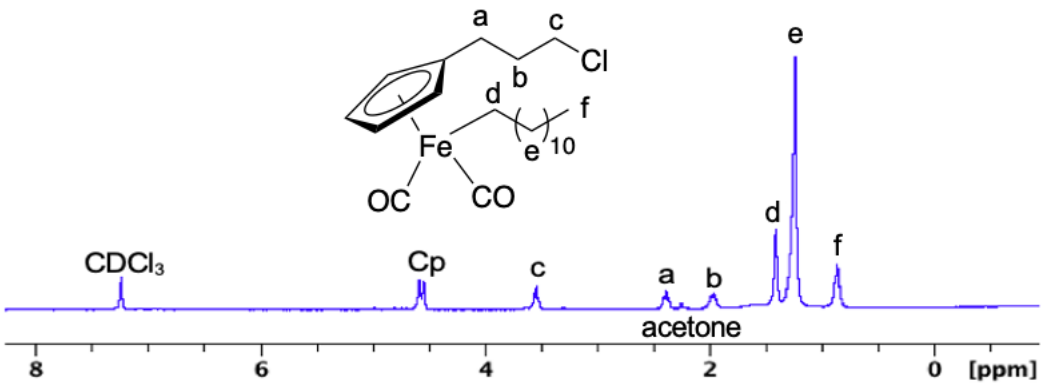

Figure 3.2. ^{1}H NMR ($CDCl_3$) spectra of $^{Cl}FpC_{12}$.

Finally, $^{P}FpC_{12}$ was synthesized *via* the reaction of $^{Cl}FpC_{12}$ with sodium diphenylphosphide at 23 °C in THF (Scheme 3.3). The solution gradually turned from yellow to orange. After reacting for 2 hours, THF was removed under vacuum, which yielded an orange oil. The crude product was purified by using Celite and silica gel column. The purified product was characterized by ^{1}H NMR and ^{31}P NMR and the resultant spectra are displayed in Figure 3. As shown in Figure 3a, the signals at 4.55 ppm and 4.47 ppm correspond to the protons in the Cp ring.[30] The signals at 7.5-7.0 ppm can be attributed to the phenyl groups.[30] Signal a, b, and c at 2.06, 1.65, and 2.33 ppm, respectively, can be assigned to the protons on the alkyl spacer connecting Cp and Cl.[30] The three signals, including *d*, *e*, and *f* at 1.39-0.86 ppm, correspond to the protons from the dodecyl chain.[30] The proton integration ratio of Ph/Cp/a/b/c/(d+e)/f is 10/4/2/2/2/22/3, which matches the expected value for $^{P}FpC_{12}$. The ^{31}P NMR spectrum (Figure 3.3 (b)) shows a signal at -15.7 ppm, which indicates the presence of a phosphine in the monomer.[18] These NMR analyses indicate that the monomer of $^{P}FpC_{12}$ was synthesized. $^{P}FpC_{18}$ was synthesized and characterized in the same manner as $^{P}FpC_{12}$. The resulting spectra are shown in the Appendix.

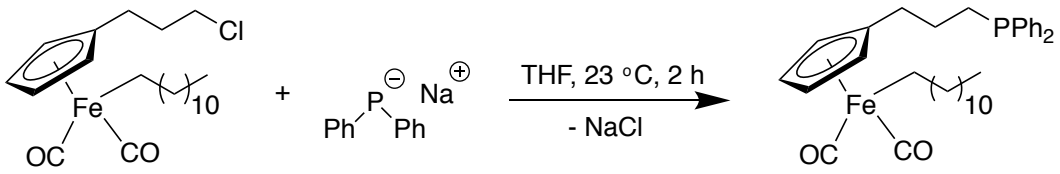

Scheme 3.3. Schematic illustration for the synthesis of $^{P}FpC_{12}$.

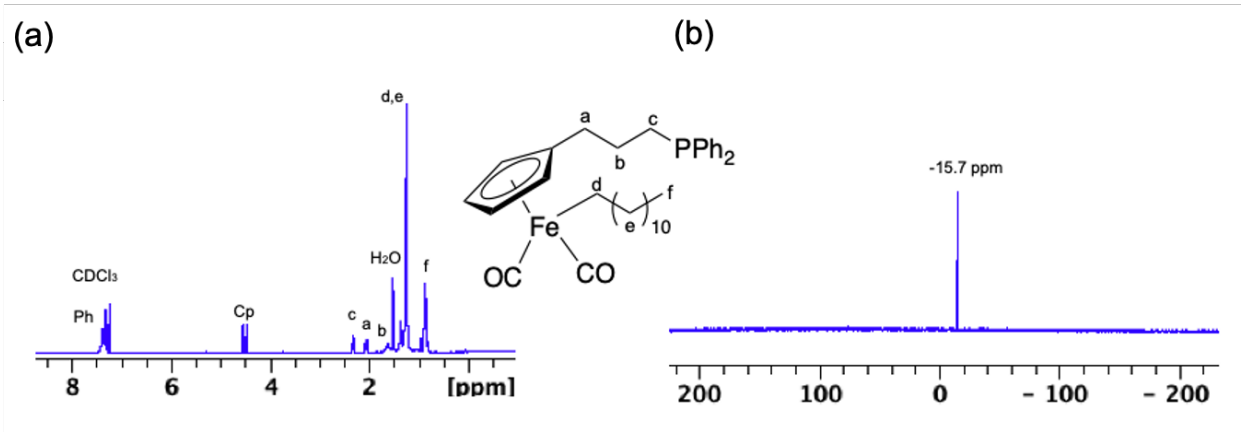

Figure 3.3. (a) ^{1}H NMR ($CDCl_3$) spectra and (b) ^{31}P NMR ($CDCl_3$) spectra of $^{P}FpC_{12}$

3.2 MIP of $^{P}FpC_x$ (X = 12, 18)

3.2.1 Bulk MIP of $^{P}FpC_x$ (X = 12, 18)

The MIP of $^{P}FpC_{12}$ was first performed at 50 °C. Aliquots were taken at certain time intervals and dissolved in $CDCl_3$ for the ^{31}P NMR analysis. The resulting spectra are presented in Figure 3.4. As shown in the figure, the signal at -15.7 ppm is attributed to the phosphorous atom in the monomer.[18] This peak gradually disappears after 18 hours, implying the consumption of the monomer. Meanwhile, the signals at -15.4 ppm and 72.7 ppm appear. These two signals are due to the phosphine end group (-15.4 ppm) and coordinated phosphorus (72.7 ppm) of linear Fp-based oligomers.[19] Therefore, the appearance of these two signals accompanied with the monomer consumption indicates that the MIP generates linear oligomers. The intensities for the signals due

to oligomers (-15.4 and 72.7 ppm) increase rapidly over 4-6 hours, and then gradually decrease relative to the other peaks. It suggests that the MIP produces oligomers at the early stage. The signals due to the oligomers (-15.4 and 72.7 ppm) completely disappeared at 120 hours, which indicates that the produced oligomers are involved in the further reaction. It is noticed that the signals at 71.6 ppm and 72.5 ppm start to appear at 2 and 4 hours, respectively. The former is attributed to the small ring produced *via* cyclization of the monomer molecule, while the latter results from the formation of P(^{P}FpC$_{12}$)$_n$ macrocycles.[30,41] Therefore, the disappearance of the oligomers is due to the cyclization. The intensities for the signal due to the small ring (71.6 ppm) relative to the macrocycles (72.5 ppm) are stronger at the early stage of the MIP and become weaker as the MIP progresses. The integration ratio for these two peaks (71.6 ppm/72.5 ppm) at 120 hours is 1/3.5, which suggests that 78% of the monomers was converted to macrocycles.

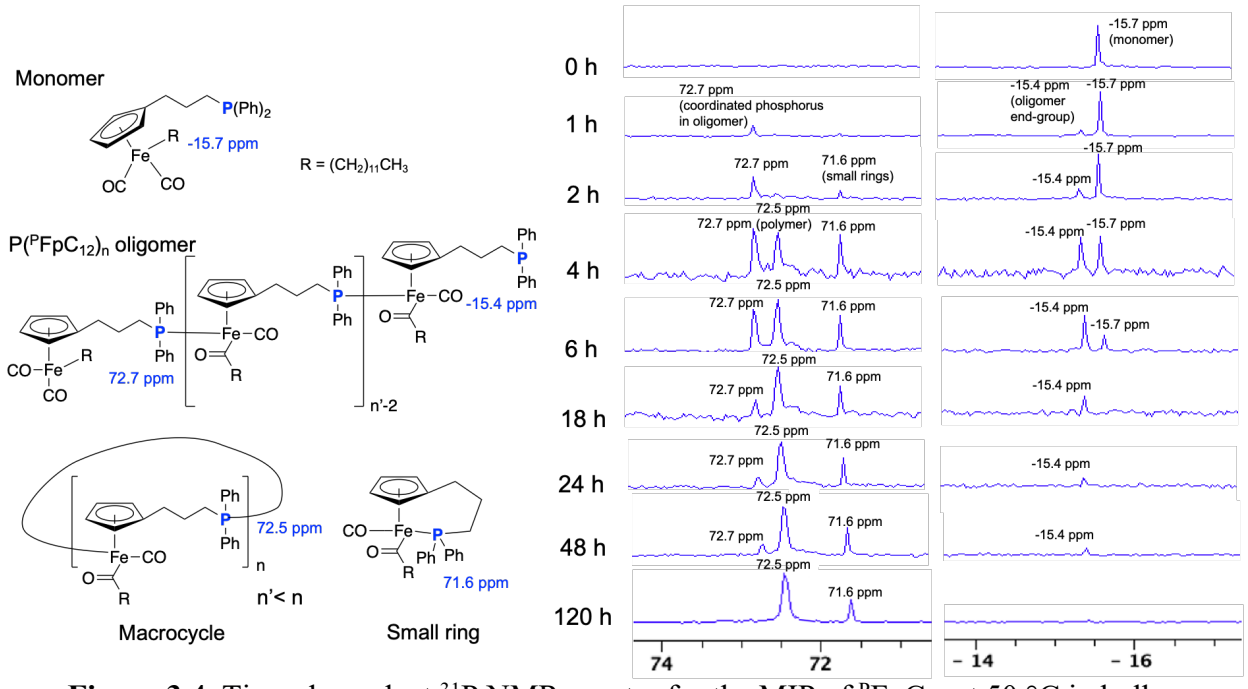

Figure 3.4. Time-dependent ^{31}P NMR spectra for the MIP of ^{P}FpC$_{12}$ at 50 °C in bulk.

The MIP of $^{P}FpC_{12}$ was also performed at 70 °C to examine the effect of temperature. The ^{31}P NMR spectra for the aliquots taken at certain time intervals are shown in Figure 3.5. As shown in the figure, the signal at -15.7 ppm due to the monomer.[18] disappears after 1 hour of the polymerization, indicating the complete consumption of the monomers. Meanwhile, the two signals appear, which are due to the phosphine end group (-15.4 ppm) and coordinated phosphorous (72.7 ppm) of $^{P}FpC_{12}$ oligomers.[19] The intensities of these signals increase rapidly in the first hour, and then gradually weaken relative to the other peaks. It suggests that the MIP at the early stage produces oligomers. The signals due to macrocycles and small rings, 72.5 ppm and 71.6 ppm,[30,31] also appear in the first hour. The intensities for the signal due to the small ring relative to the macrocycles are stronger at the first hour and become weaker as the polymerization progresses. This suggests that the disappearance of the oligomers is due to the cyclization. The minimum polymerization time required is 24 hours, which is significantly faster than the time required in the bulk at 50 °C (120 hours). The integration ratio for these two peaks (71.6 ppm/72.5 ppm) at 24 hours is 1/3.2, which suggests 75% of the monomer is converted to macrocycles.

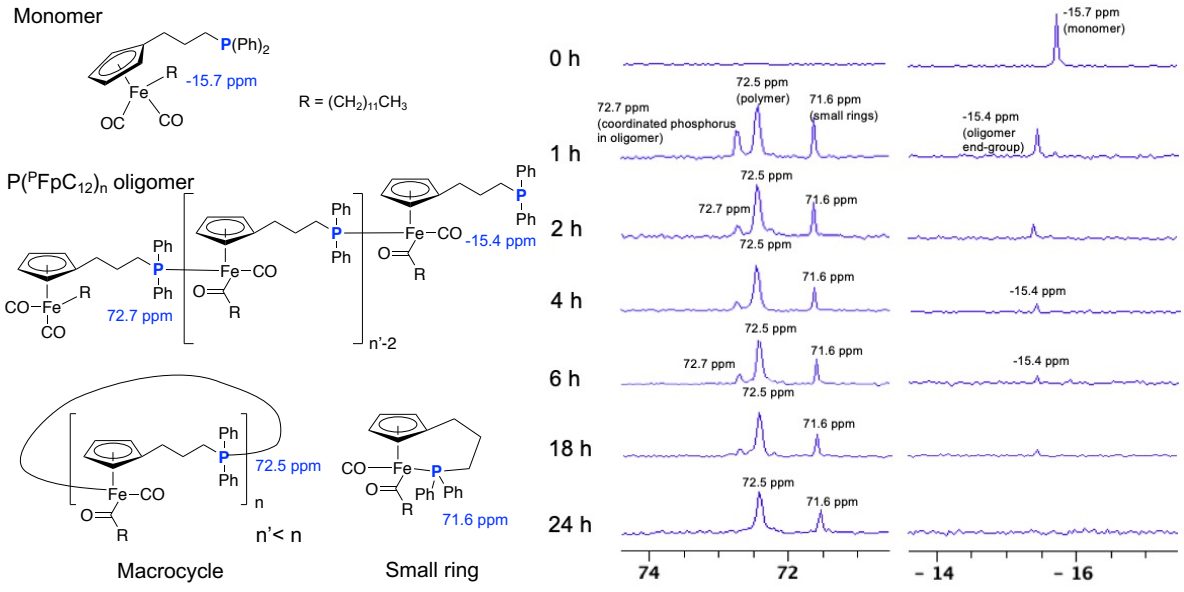

Figure 3.5. Time-dependent ^{31}P NMR spectra for the MIP of $^{P}FpC_{12}$ at 70 °C in bulk.

By further increasing temperature to 100 °C, the polymerization rate increased significantly. The monomer is consumed completely after 1 hour as indicated by the disappearance of the signal at -15.7 ppm due to the monomer (Figure 3.6).[18] The absence of signals at -15.4 and 72.7 ppm implies that no oligomers remain at 1 hour due to the faster reaction at 100 °C.[19] All oligomers are cyclized into macrocycles in the first hour of polymerization. Signals at 72.5 ppm and 71.6 ppm (Figure 3.6) are assigned to the phosphorus atoms in the macrocycle and cyclized monomer.[30,31] These two signals appear in the first hour, indicating the occurrence of the ring-closing MIP and monomer cyclization at the early stage of the polymerization. The intensity of the small rings is more significant in the spectra for the MIP performed at 100 °C than those at 50 °C and 70 °C, suggesting that the monomer cyclization is favored at 100 °C. The integration ratio for these two peaks (71.6 ppm/72.5 ppm) at 2 hours is 1/1.9, which suggests that 65% of the monomer is converted to macrocycles.

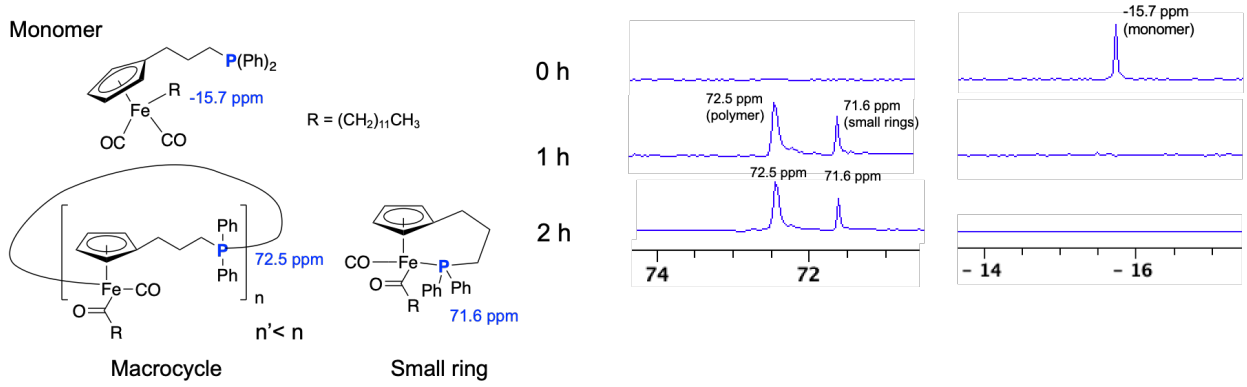

Figure 3.6. Time-dependent ^{31}P NMR spectra for the MIP of $^{P}FpC_{12}$ at 100 °C in bulk.

The MIP of $^{P}FpC_{18}$ was performed at 70 and 100 °C in the bulk to study the effect of a longer alkyl chain on the polymerization. The aliquots of the polymerization system at 70 °C were taken at certain time intervals and analyzed by ^{31}P NMR, and the resulting spectra are shown in Figure 3.7. As shown in the figure, the signal at -15.7 ppm due to the monomers disappears in 2

hours, implying the consumption of monomers.[18] Meanwhile, the intensities for the two signals (-15.4 ppm and 72.7 ppm) due to the phosphine end group and coordinated phosphorous[16] increase rapidly in the first hour and then gradually weaken relative to the other peaks, because the MIP produces oligomers at the early stage. The signals (72.5 ppm and 71.6 ppm) due to macrocycles and small rings[30,31] also appear in the first hour. The intensities for the signal due to the small ring relative to the macrocycles are stronger at the first hour and become weaker as the polymerization progresses. This suggests that the disappearance of the oligomers is due to the cyclization. The integration ratio for these two peaks (71.6 ppm/72.5 ppm) at 24 hours is 1/4.0, which suggests that 80% of the monomer is converted to macrocycles.

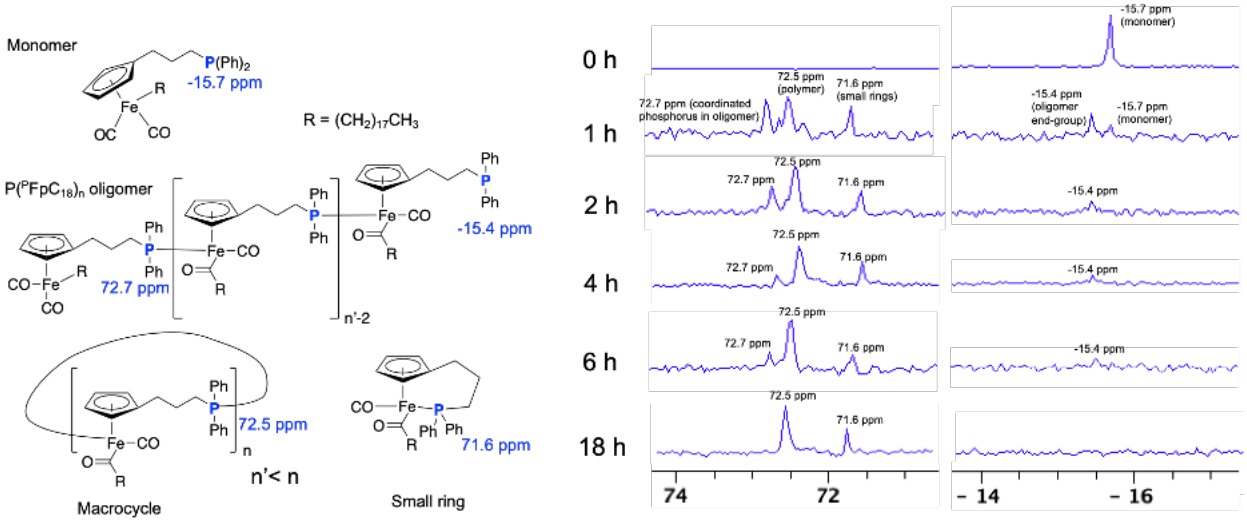

Figure 3.7. Time-dependent ^{31}P NMR spectra for the MIP of $^{P}FpC_{18}$ at 70 °C in bulk.

The MIP of $^{P}FpC_{18}$ was performed at 100 °C and aliquots were taken at certain intervals and analyzed by ^{31}P NMR. The resulting spectra are shown in Figure 3.8. The signal at -15.7 ppm due to the monomer[18] disappears after 1 hour of polymerization, suggesting the consumption of monomers. Meanwhile, the two signals that are due to the phosphine end group (-15.4 ppm) [19] and coordinated phosphorous (72.7 ppm)[19] of $^{P}FpC_{18}$ oligomer appear in the first hour and disappear after 2 hours. The disappearance of these two peaks with increased macrocycles signal (72.5

ppm)[31] suggests the cyclization of the oligomers. The integration ratio for these two peaks (71.6 ppm/72.5 ppm) at 18 hours is 1/3.0, which suggests that 75% of the monomer is converted to macrocycles.

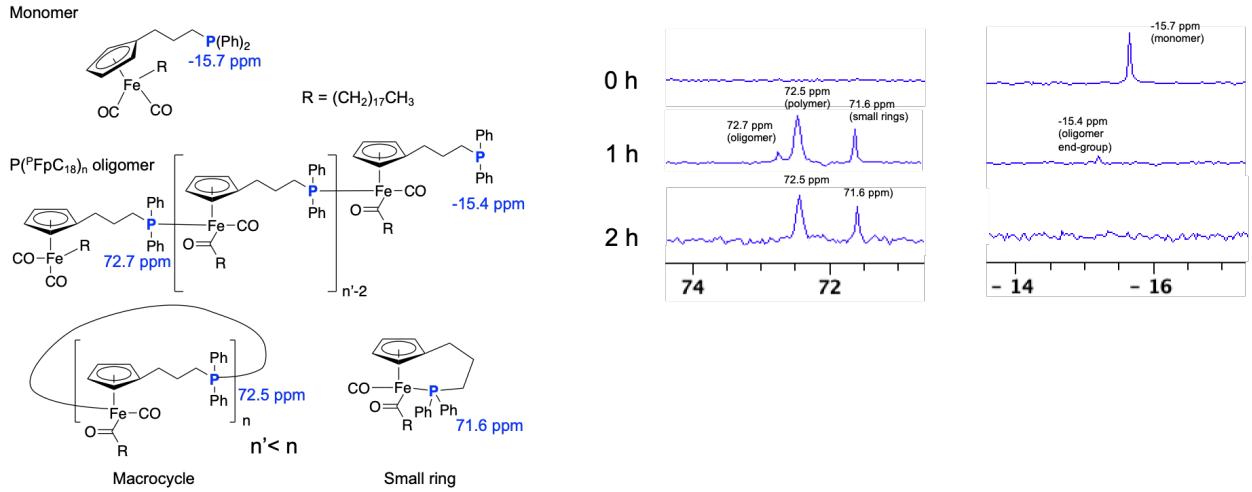

Figure 3.8. Time-dependent ^{31}P NMR spectra for the MIP of $^{P}FpC_{18}$ at 100 °C in bulk

3.2.2. Solution MIP of $^{P}FpC_{x}$ (n = 12, 18)

The effect of temperature on the MIP of $^{P}FpC_{x}$ (n = 12, 18) in solution was studied. The MIP of $^{P}FpC_{12}$ was first performed at 70 °C in 50% toluene or THF and aliquots were taken at certain time intervals and analyzed by ^{31}P NMR. The resulting spectra are illustrated in Figure 3.9 and 3.10. Disappearance of signal at -15.8 ppm after 2 hours suggests the consumption of the monomers. Meanwhile, signals at -15.4 ppm and 72.7 ppm due to the formation of the linear oligomer[19] appear in the first hour, and then gradually weaken relative to the other peaks. Both macrocycles and cyclized monomers are produced within the first hour, as indicated by the appearance of the signals at 72.5 ppm and 71.6 ppm.[30,31] These oligomer signals completely vanish after 18 hours, implying that all linear oligomers were cyclized, and macrocycles were formed. The integration ratio for these two peaks (71.6 ppm/72.5 ppm) at 18 hours in THF or toluene are

1/3.5 and 1/3.8, respectively, which suggests that 77% and 79% of the monomer are converted to macrocycles.

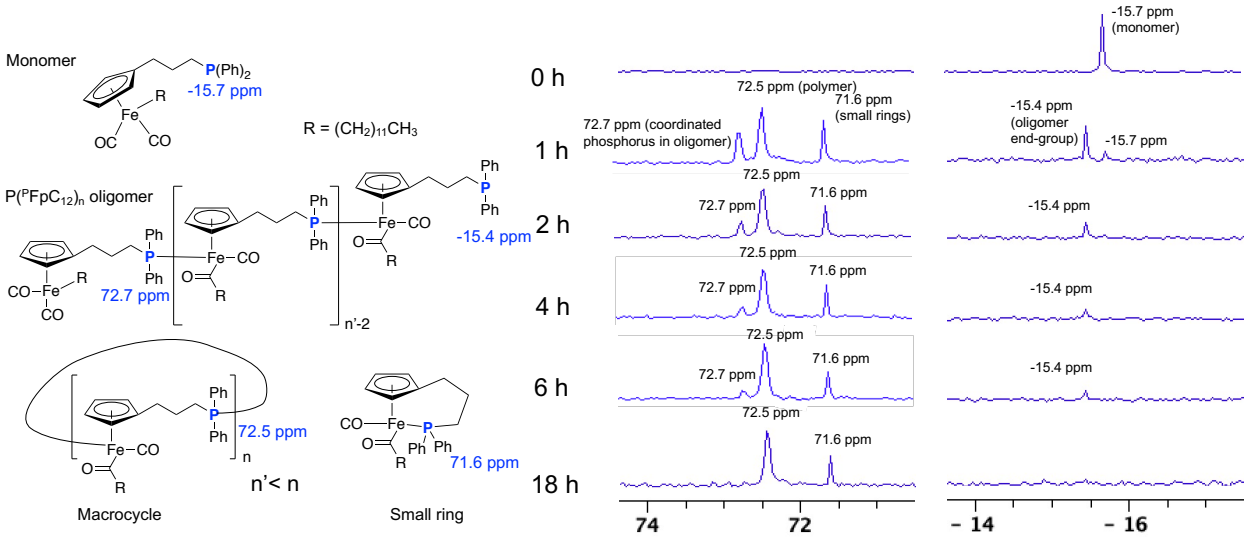

Figure 3.9. Time-dependent ^{31}P NMR spectra for the MIP of $^{P}FpC_{12}$ at 70 °C in THF with 50% wt concentration.

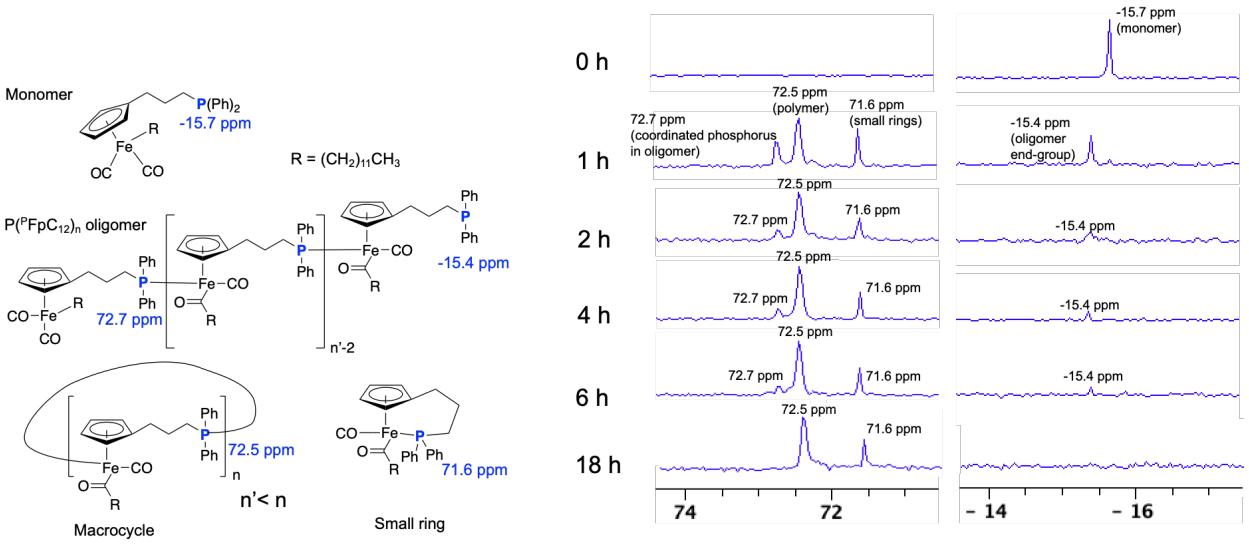

Figure 3.10. Time-dependent ^{31}P NMR spectra for the MIP of $^{P}FpC_{12}$ at 70 °C in toluene with 50% wt concentration.

The MIP of $^{P}FpC_{12}$ was performed at 100 °C in toluene (50% wt) and aliquots were taken at certain intervals and analyzed by ^{31}P NMR. The resulting spectra are shown in Figure 3.11. The monomer signal at -15.7 ppm[18] disappears after 1 hour of polymerization, suggesting the consumption of monomers. The signals due to macrocycles and small rings, at 72.5 ppm and 71.6 ppm,[30,31] respectively, also appear in the first hour. The integration ratio for these two peaks (71.6 ppm/72.5 ppm) at 2 hours is 1/2.0, which suggests that 67% of the monomer is converted to macrocycles.

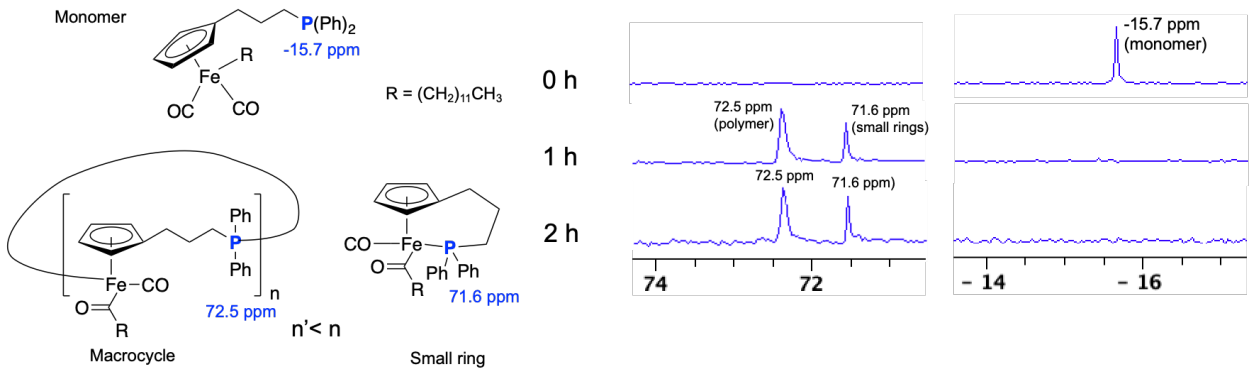

Figure 3.11. Time-dependent ^{31}P NMR spectra for the MIP of $^{P}FpC_{12}$ at 100 °C in toluene with 50% wt concentration.

The MIP of $^{P}FpC_{18}$ was performed at 70 °C in 50% toluene to study the effect of different alkyl chain length for solution polymerization. The aliquots were taken at certain time intervals and analyzed by ^{31}P NMR. The resulting spectra are presented in Figure 3.12. The disappearance of signal at -15.8 ppm after 2 hours suggests the consumption of the monomers.[18] Meanwhile, the signals at -15.4 ppm and 72.7 ppm due to the linear oligomer[19] appear in the first hour, and then gradually weaken relative to the other peaks. The signals at 72.5 ppm and 71.6 ppm due to, respectively, macrocycles and cyclized monomers[30,31] are generated within the first hour. These oligomer signals completely vanish after 18 hours, implying that all linear oligomers were

cyclized, and macrocycles were formed. The integration ratio for these two peaks (71.6 ppm/72.5 ppm) at 18 hours is 1/2.5, which suggests that 76% of monomer is converted to macrocycles.

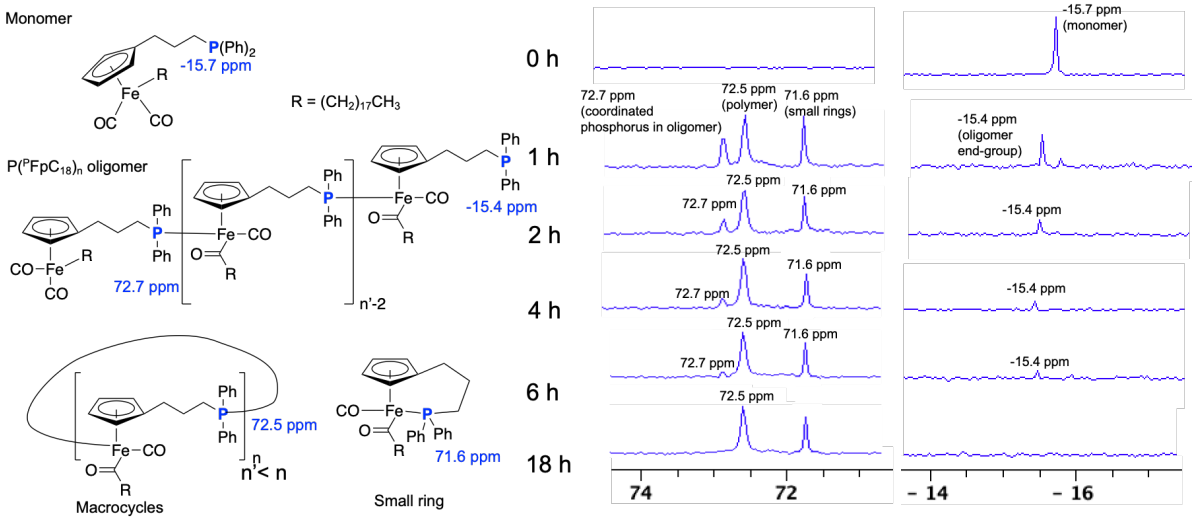

Figure 3.12. Time-dependent ^{31}P NMR spectra for the MIP of $^{P}FpC_{18}$ at 70 °C in toluene with 50% wt concentration.

The MIP of $^{P}FpC_{18}$ was performed at 100 °C in toluene (50% wt) and aliquots were taken at certain intervals and analyzed by ^{31}P NMR. The resulting spectra are shown in Figure 3.13. Monomer signal at -15.7 ppm[18] disappears after 1 hour of polymerization, suggesting the consumption of monomers. The signals due to macrocycles and small rings appearing at, respectively, 72.5 ppm and 71.6 ppm,[30,31] also appear in the first hour. The integration ratio for these two peaks (71.6 ppm/72.5 ppm) at 2 hours is 1/2.1, which suggest that 68% of monomer is converted to macrocycles.

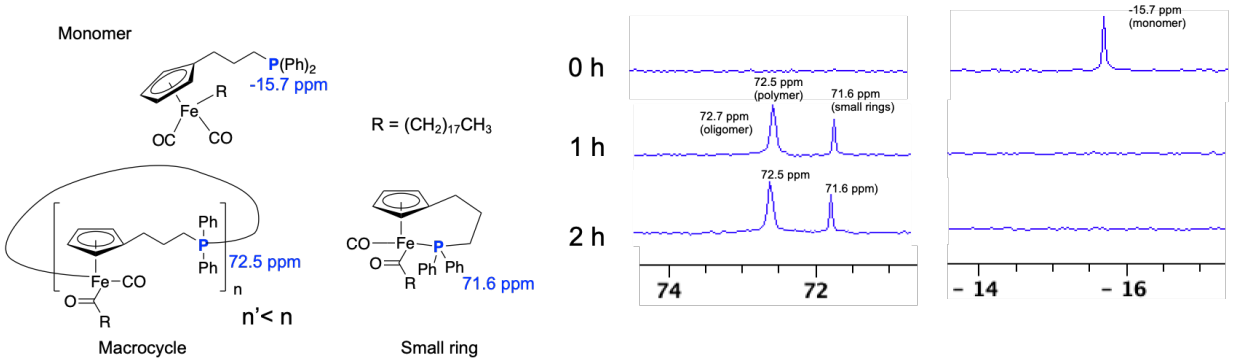

Figure 3.13. Time-dependent ^{31}P NMR spectra for the MIP of $^{P}FpC_{18}$ at 100 °C in toluene with 50% wt concentration.

The yields obtained under different conditions at various conditions are compared in Table 3.1. Both bulk and solution MIP produce less macrocycles at a higher polymerization temperature (100 °C). The yields are similar when MIP is performed in solution but become dependent on the alkyl chain in the monomers in bulk MIP. A larger yield is produced from the bulk MIP of $P(^{P}FpC_{18})_n$, which probably is caused by the larger steric hindrance of the longer chains (C_{18}), which suppresses monomer cyclization.

Table 3.1. The yields of $P(^{P}FpC_x)_n$ macrocycles synthesized *via* MIP under varied conditions.

	Bulk MIP			Solution MIP		
	50 ºC	70 ºC	100 ºC	70 ºC (THF)	70 ºC (Toluene)	100 ºC (Toluene)
$P(^{P}FpC_{12})_n$	78 %	75 %	65 %	77 %	79 %	67 %
$P(^{P}FpC_{18})_n$		80 %	75 %		76 %	68 %

3.2.3 Purification of the resultant macrocycles

MIP of $^{P}FpC_{12}$ was performed in the bulk at 70°C.[30] The colour of the polymerization system gradually turned from light orange to reddish-brown. After 48 hours, the polymerization

was terminated by cooling the reaction flask to 23 °C. The crude products were first dissolved in a minimum amount of THF (0.2 mL). This THF solution was added to hexane (80 mL) at 23 °C and precipitation was observed. However, the supernatant remained turbid even when the solution was left overnight, which suggests the presence of some macromolecules in the supernatant.

The products extracted from the supernatant were characterized by ^{31}P NMR analysis. The resultant spectrum shows a significant peak at 72.5 ppm (Figure 3.14 (a)) that has been assigned to the macrocycles of P(^{P}FpR)$_n$.[27] Another peak at 71.6 nm is attributed to the phosphorus in the small ring produced *via* the intramolecular cyclization of the monomers.[28] Hexane is able to precipitate P(^{P}FpC$_6$)$_n$ as we have reported.[1] However, P(^{P}FpC$_{12}$)$_n$ products have a longer alkyl chain, which may endow the product a better solubility in THF/hexane mixed solvents and thus become more difficult to precipitate. Therefore, we tried to use cold hexane for the precipitation.

Figure 3.14. ^{31}P NMR ($CDCl_3$) spectra for the products extracted from the supernatant. (a) hexane (23ºC), (b) hexane (-50 ºC), (c) methanol (-50 ºC), (d) diethyl ether (-50 ºC) (e) ethanol (-50 ºC) was used for the precipitation.

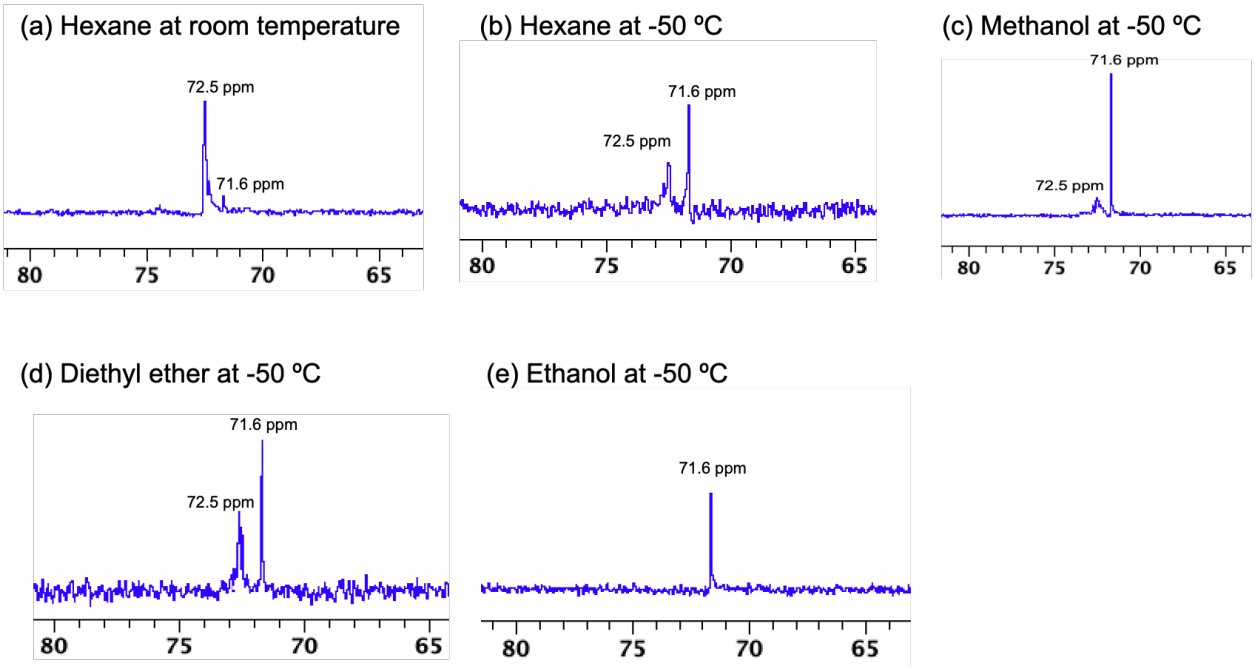

Hexane was first cooled to -50 °C, then the THF solution of the products was added dropwise to the cold hexane and precipitation was observed. The supernatant is also turbid even after leaving the solution overnight in -50°C freezer, which suggests the presence of some macromolecules in the supernatant. The ^{31}P NMR analysis of the products extracted from the supernatant also shows a peak at 72.5 ppm (Figure 3.14 (b)) due to the phosphorus in the macrocycles.[30] However, this signal is fairly weaker than that in Figure 3.14 (a). A stronger signal for the peak at 71.6 ppm due to the cyclized monomers is observed (Figure 3.14 (b)).[31] This result indicates that the precipitation using cold hexane helps to separate the macrocycles from the small ring, but still not effectively.

We also tried to use cold diethyl ether and cold methanol for the precipitation. The ^{31}P NMR analysis of the products extracted from the supernatants also show the presence of the macrocycles (Figure 3.14 (c) and 3.14 (b)). However, we found that the supernatant resulting from the precipitation using methanol (-50 °C) is a clear solution, which suggests that the alcohol is a better solvent for the precipitation. The macrocycles consist of the polar backbone with Fp repeating units and non-polar pendent groups of dodecyl chains. Methanol is a polar solvent which interact with the polar backbone, leading to a slight solubility in the supernatant with methanol/THF mixed solvents. Therefore, we tried to use cold ethanol, a less polar alcohol, for the precipitation. The supernatant was a clear solution. The ^{31}P NMR analysis of the products extracted from the supernatant is shown in Figure 3.14c. As shown in the figure, the spectrum shows a single peak at 71.6 ppm due to the small rings (Figure 3.14 e). The absence of the signal at 72.5 ppm suggested that no macrocycles remained in the supernatant. Thus, cold ethanol effectively separates the macrocycles from the small rings.

$^{P}FpC_{18}$ with an octadecyl chain was synthesized and characterized by the same techniques used for $^{P}FpC_{12}$. MIP of $^{P}FpC_{18}$ was performed in the bulk at 70°C.[30] After 48 hours, the polymerization was terminated by cooling the reaction flask to room temperature. The crude products were first dissolved in a minimum amount of THF (0.2 mL). This THF solution was added to cold methanol (-50 °C). However, the supernatant remained turbid, and no precipitation was observed. It was expected that $P(^{P}FpC_{18})_n$ would be easier to be precipitated in methanol, because the macrocycles, compared with $P(^{P}FpC_{12})_n$, have a longer non-polar pendent group. The observed abnormal behaviour could be related to the molecular weight.

However, upon a centrifugation, we separated the solid from the supernatant, which became clear. The separated solid and the products extracted from the supernatant were characterized by ^{31}P NMR. The resultant spectrum from the separated solid (Figure 3.15 (a)) shows a single peak at 72.5 ppm, suggesting the presence of macrocycles. The ^{31}P NMR analysis of the products extracted from the supernatant (Figure 3.15 (b)) shows a single peak due to small rings. The absence of the signal at 72.5 ppm implies that no macrocycle remains in the supernatant. Therefore, cold methanol with centrifugation effectively separates the macrocycles from the small rings.

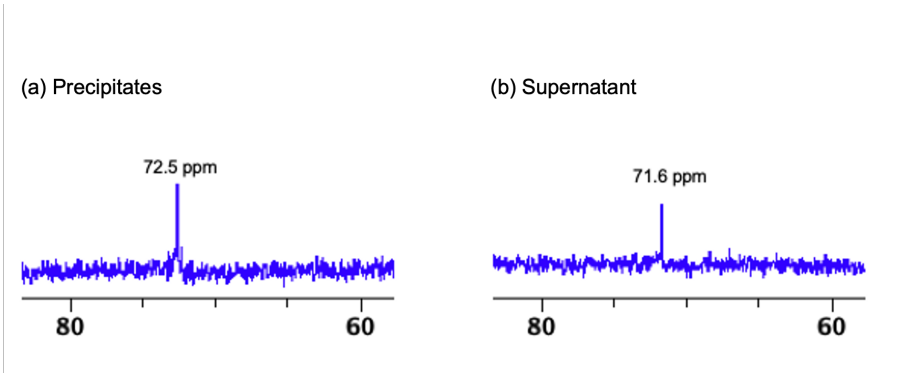

Figure 3.15. ^{31}P NMR ($CDCl_3$) spectra for (a) precipitates and (b) the products extracted from the supernatant.

3.2.4 Characterization of P(^{P}FpC$_{X}$)$_{n}$ (X = 12 or 18)

P(^{P}FpC$_{12}$)$_{n}$ was synthesized *via* MIP of ^{P}FpC$_{12}$ in the bulk. The resulting products were characterized by ^{1}H NMR and ^{31}P NMR and the resultant spectra are displayed in Figure 3.16. As shown in Figure 3.16 (a), the signals at 7.25-7.38 ppm can be attributed to the phenyl groups.[30] The signals at 4.08-3.95 correspond to the protons in the Cp ring. Signals *a*, *b*, and *c* at 1.63, 2.12, and 2.25 ppm in Figure 15a can be assigned to the protons in the propyl diphenylphosphine. Signals *d*, *e*, and *f* at 2.76, 2.52, and 0.83 ppm can be attributed to the protons in the pendent acyl groups. The ^{31}P NMR spectrum (Figure 3.16 (b)) shows a signal at 72.5 ppm, which indicates the presence of the macrocycles.[30] These NMR analyses imply that P(^{P}FpC$_{12}$)$_{n}$ was synthesized.

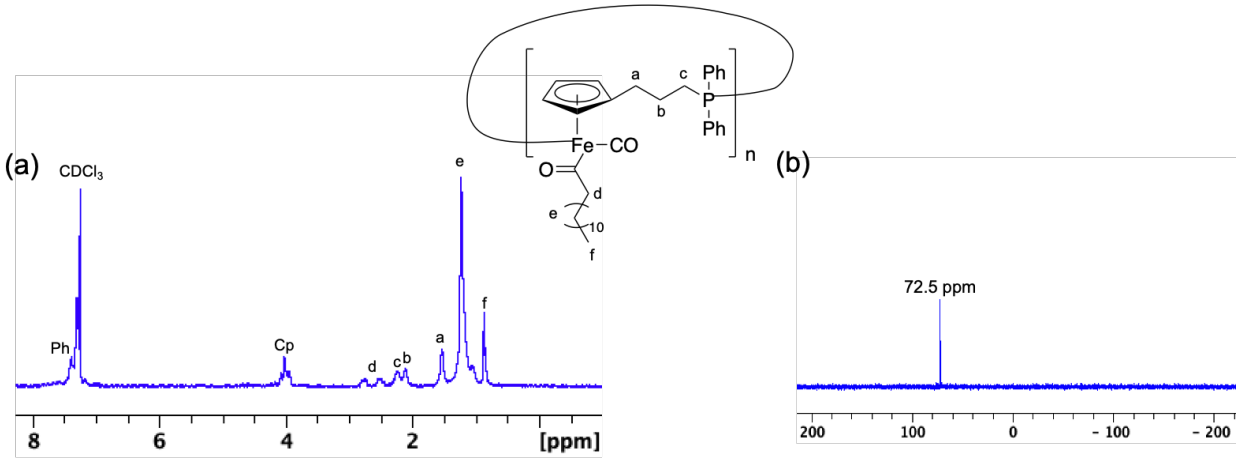

Figure 3.16. (a) ^{1}H NMR ($CDCl_3$) spectra and (b) ^{31}P NMR ($CDCl_3$) spectra of P(^{P}FpC$_{12}$)$_{n}$ macrocycles

The solutions of P(^{P}FpC$_{12}$)$_{n}$ and P(^{P}FpC$_{18}$)$_{n}$ in THF (1.0 mg/mL) were prepared and analyzed by dynamic light scattering (DLS). As shown in Figure 3.17 (a)-(b), the DLS curve for P(^{P}FpC$_{12}$)$_{n}$ and P(^{P}FpC$_{18}$)$_{n}$ macrocycles show two populations for the solutions (P(^{P}FpC$_{12}$)$_{n}$ with D_h = 135.5 and 4.21 nm and P(^{P}FpC$_{18}$)$_{n}$ with D_h = 58.8 and 4.14 nm). The DLS profiles based on number are shown as Figure 3.17 (c)-(d), which only reveal one peak with D_h of 4.22 nm and 4.32 nm for the solutions of P(^{P}FpC$_{12}$)$_{n}$ and P(^{P}FpC$_{18}$)$_{n}$, respectively. The DLS analysis suggests that

both molecules are soluble in THF with the molecular size of *ca*. 4 nm, but they tend to aggregate forming a small number of aggregates.

The transmission electron microscope (TEM) images for the two molecules are displayed in Figure 3.17 (e)-(f). The TEM samples were prepared by adding a drop of $P(^{P}FpC_X)_n$ solution (1 mg/mL) on a copper grid substrate and then leaving in air overnight before experiment. As shown in Figure 3.17 (e), cyclic structures with white centers of *ca.* 5-10 nm in diameters are observed. The contrast was caused by the rupture of the carbon film in the center of the rings after exposing the grid to the electron beam for a few minutes.[27] Rings with diameters of *ca.* 5-10 nm and 20-30 nm were observed in Figure 3.18 (f).

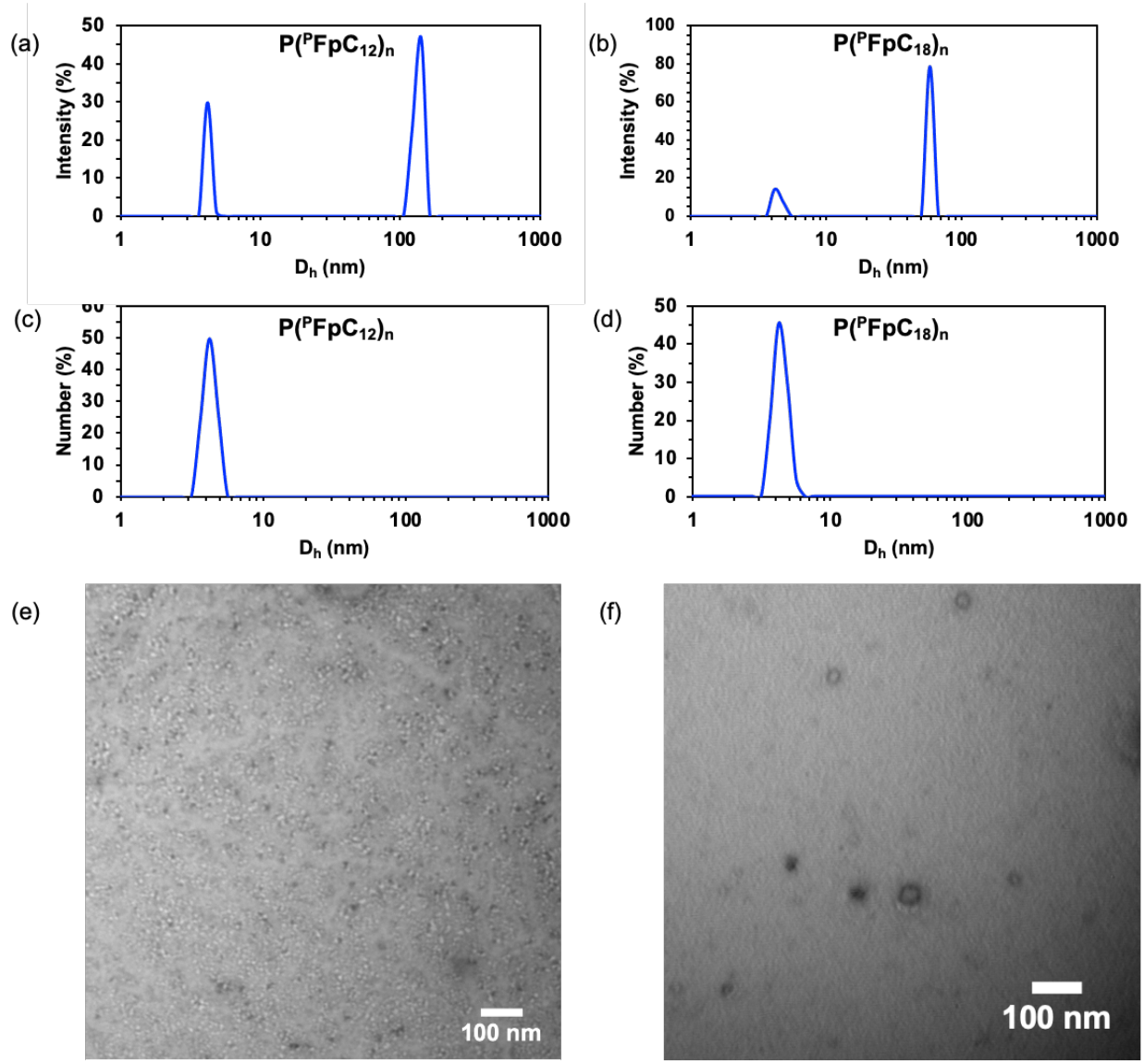

Figure 3.17. DLS profiles (a) by scattering intensity for the solution of $P(^{P}FpC_{12})_n$ in THF and (b) $P(^{P}FpC_{18})_n$ in THF, (c) by molecular numbers for the solution of $P(^{P}FpC_{12})_n$ in THF and (d) $P(^{P}FpC_{18})_n$ in THF. TEM images of (e) $P(^{P}FpC_{12})_n$ and (f) $P(^{P}FpC_{18})_n$. The TEM sample was prepared by drying a drop of the THF solutions on the copper grid covered by a carbon film. The concentrations for all the solutions are 1.0 mg/mL.

3.2.5 Solubility test of P(^{P}FpC$_{X}$)$_{n}$ (X = 12 or 18)

The MIP of ^{P}FpC$_{12}$ and ^{P}FpC$_{18}$ was performed at 70 °C and the resultant macrocycles was dissolved in various solvents at 23 °C. The resulting data are summarized in Table 3.1. Both P(^{P}FpC$_{12}$)$_{n}$ and P(^{P}FpC$_{18}$)$_{n}$ could not dissolve in DMF, DMSO, and methanol. When P(^{P}FpC$_{12}$)$_{n}$ and P(^{P}FpC$_{18}$)$_{n}$ were dissolved in toluene or THF, a clear solution was observed, suggesting good solubility in the solvents. Only P(^{P}FpC$_{18}$)$_{n}$ is soluble in hexane due the longer alkyl chain that results in a better solubility in non-polar solvent.

Table 3.2. Solubility test of P(^{P}FpC$_{12}$). The concentration is 1.0 mg/mL for the solution.

	Hexane	Toluene	THF	DMF	DMSO	Methanol
P(^{P}FpC$_{12}$)$_{n}$	×	✓	✓	×	×	×
P(^{P}FpC$_{18}$)$_{n}$	✓	✓	✓	×	×	×

3.3 Self-assembly of P(^{P}FpC$_{x}$)$_{n}$ (x = 12 or 18)

P(^{P}FpC$_{12}$)$_{n}$, synthesized in the bulk at 100 °C, was first dissolved in THF (1 mg/mL), various poor solvents (10 mL) were added instantaneously into the THF solution to study the effect of poor solvents on the self-assembly. The prepared solutions were characterized by DLS and the resulting data for P(^{P}FpC$_{12}$)$_{n}$ are shown in Table 3.3. As shown in Table 3.3, when DMF is used as a poor solvent, there is no sufficient light scattering signal suggesting no particles were formed. When methanol and water are used as poor solvents, P(^{P}FpC$_{12}$)$_{n}$ seems able to self-assemble, but leads to precipitation after aging. When DMSO was added to the THF solution, P(^{P}FpC$_{12}$)$_{n}$ macrocycles self-assemble into colloids with D_h of 285 nm. The colloids keep growing to 329 nm upon aging the solution for 7 days and then become stable. P(^{P}FpC$_{6}$)$_{n}$ is able to self-assemble in THF/hexane mixed solvents as we have reported.[37] Therefore, we expected that P(^{P}FpC$_{12}$)$_{n}$ could also self-assemble in the mixed solvents. As shown in Table 3.3, P(^{P}FpC$_{12}$)$_{n}$ assembles into colloids in hexane/THF (10/1, 8.5/1.5) with D_h of 444 and 421 nm, respectively. However, upon

aging the solutions, the colloids precipitate. When the ratio of hexane/THF is 8/2, the DLS of the freshly prepared solution indicates the formation of assemblies with D_h of 490 nm. However, the light scattering becomes very weak after the solution is aged for 3 days. It suggests that the aggregates gradually disassemble during the aging. No assemblies are formed in the mixed solvents with hexane/THF ratio of 7/3, due to a good solubility of the molecules.

Table 3.3. Self-assembly of $P(^{P}FpC_{12})_n$ with varied poor solvents. 1 mg of $P(^{P}FpC_{12})_n$ was first dissolved in THF and various poor solvents were added instantaneously to the THF solution.

Poor solvent (THF : poor solvent)	D_h/PDI	After 3 days	After 7 days	After 14 days
DMF (1:10)	N/A*			
Methanol (1:10)	820.9/0.278	precipitate		
Water (1:10)	305.9/0.236	precipitate		
DMSO (1:10)	285.0/0.002	314.7/0.039	329.3/0.039	328.7/0.065
Hexane (1:10)	443.8/0.190	precipitate		
Hexane (1.5:8.5)	420.5/0.373	precipitate		
Hexane (2:8)	490/0.563**	N/A*		
Hexane (3:7)	N/A*			

*Low count rate (<5), $P(^{P}FpC_{12})_n$ remain soluble in the solution
** Low count rate (10-100)

The data for the self-assembly of $P(^{P}FpC_{18})_n$ are displayed in Table 3.4. As shown in Table 3.4, when DMF is used as a poor solvent, there is no sufficient light scattering signal suggesting no particles were formed. When methanol and water are used as poor solvent, $P(^{P}FpC_{18})_n$ seems able to self-assemble, but leads to precipitation after aging. When DMSO was added to the THF solution, $P(^{P}FpC_{18})_n$ self-assembles into colloids with D_h of 395 nm. The colloids keep growing to 494 nm upon aging the solution for 7 days and then become stable.

Table 3.4. Self-assembly of $P(^{P}FpC_{18})_n$ with varied poor solvents. 1 mg of $P(^{P}FpC_{18})_n$ was first dissolved in THF and various poor solvents were added instantaneously to the THF solution.

Poot solvent (THF : poor solvent)	D_h/PDI	After 3 days	After 7 days	After 14 days
DMF (1:10)	N/A*			
Methanol (1:10)	726.3/0.311	precipitate		
Water (1:10)	305.9/0.236	precipitate		
DMSO (1:10)	395.6/0.087	516.3/0.090	493.7/0.175	519.7/0.074

*Low count rate (<5), $P(^{P}FpC_{18})_n$ remain soluble in the solution

The assemblies of $P(^{P}FpC_{12})_n$ and $P(^{P}FpC_{18})_n$ in THF/DMSO were analyzed by TEM. The TEM samples were prepared by adding a drop of self-assembled $P(^{P}FpC_{12})_n$ and $P(^{P}FpC_{18})_n$ in DMSO solution on a copper grid substrate and leaving in air overnight before conducting the experiment. As shown in Figure 3.18, irregular structures of 200-300 nm in size are observed.

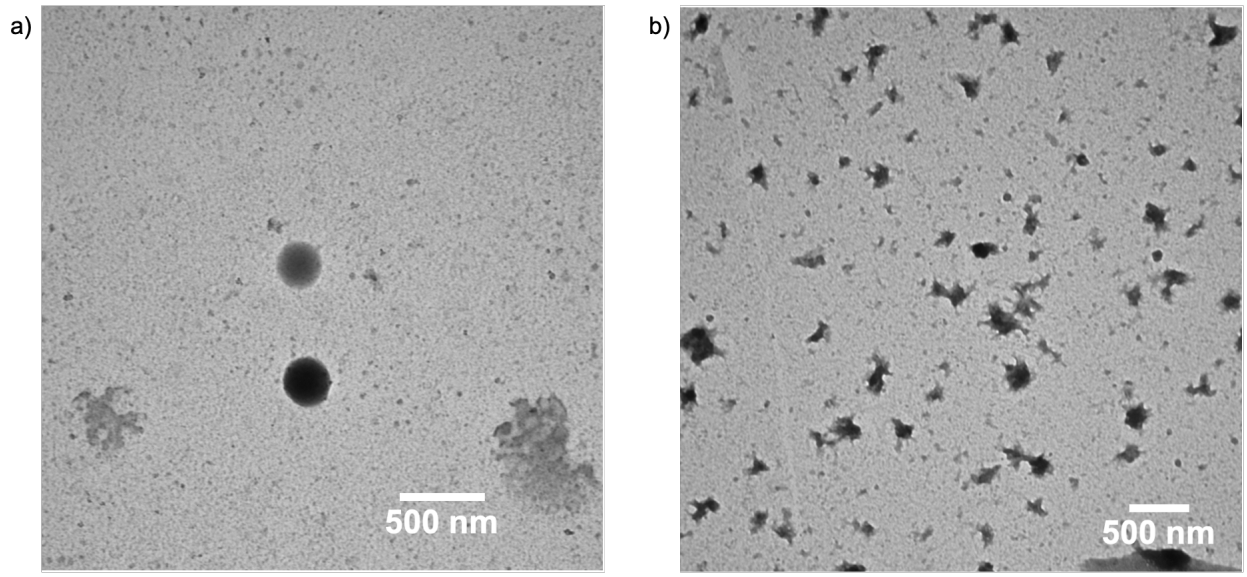

Figure 3.18. TEM images of self-assembled (a) $P(^{P}FpC_{12})_n$ and (b) $P(^{P}FpC_{18})_n$ in DMSO. Both scale bars are 500 nm.

4.0 Conclusion

In summary, Macrocycles $P(^{P}FpC_X)_n$ (x = 12, 18) were synthesized *via* Migration Insertion Polymerization (MIP) and characterized by NMR, DLS, and TEM. The $^{P}FpC_X$ (x = 12, 18) monomers underwent cyclization that produces $^{P}FpC_X$ small rings and $P(^{P}FpC_X)_n$ oligomers at the early stage of MIP, which is followed by the ring closing of the oligomer to produce macrocycles. The MIP in the bulk and solutions are similar in the polymerization rate, but much faster at a higher temperature. The yield of macrocycles is dependent on the polymerization condition and the type of monomers. Fewer macrocycles were generated at a higher temperature. The MIP of $P(^{P}FpC_{18})_n$ in the bulk generated more macrocycles as compared to the MIP of $P(^{P}FpC_{12})_n$ in the bulk. The self-assembly of $P(^{P}FpC_X)_n$ (X = 12, 18) were briefly studied. Both $P(^{P}FpC_{12})_n$ and $P(^{P}FpC_{18})_n$ can formed stable colloids in DMSO/THF mixed solvents.

5.0 Future Work

The successful synthesis of $P(^{P}FpC_{X})_{n}$ (X = 12, 18) has offered some applications in the field of supramolecular chemistry. For example, the effect of co-solvent and temperature on the self-assembly of $P(^{P}FpC_{X})_{n}$ was characterized. Moreover, the self-assembly behaviors of $^{P}FpC_{X}$ small rings that formed *via* monomer cyclization and $P(^{P}FpC_{X})_{n}$ macrocycles could be compared. ^{P}FpR monomers could be modified with a longer alkyl spacer between the Fp head group and phosphine end group. The longer alkyl spacer may allow the backbone chain to be more flexible and affect the ring size.

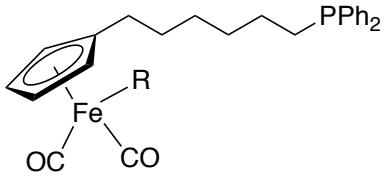

Figure 5.1. Possible modifications of ^{P}FpR monomers

References

[1] Y. Zhu N. S. Hosmane, *ChemistryOpen*, **2015**, 4, 408-417.

[2] S. J. Clarson and J. A. Semlyen, *Polymer*, **1986**, 27, 1633-16366.

[3] D. E. Lonsdale, C. A. Bell, and M. J. Monteiro, *Macromolecules,* **2010**, 43, 3331-3339.

[4] B. Zhang, H. Zhang, Y. Li, J. N. Hoskins and S. M. Grayson, *ACS Macro Lett.*, **2013**, 2, 845-848

[5] T. Isono , Y. Satoh , K. Miyachi , Y. Chen , S. Sato , K. Tajima , T. Satoh and T. Kakuchi , *Macromolecules*, **2014,** 47 , 2853-2863

[6] B. A. Laurent and S. M. Grayson *Chem. Soc. Rev.* **2009**, 38, 2202-2213.

[7] X. Tu, M. Liu and H. Wei, *J. Polym. Sci. Part A*, **2016**, 54, 1447-1458.

[8] J. N. Hoskins and S. M. Grayson, *Macromolecules,* **2009,** 42, 6406-6413.

[9] M. Kubo, T. Hayashi, H. Kobayashi, K. Tsuboi, T. Itoh, *Macromolecules*, **1997**, 30, 2805-2807.

[10] Y. Zhu and N. S. Hosmane, *ChemistryOpen*, **2015**, 4, 408-417.

[11] H. R. Kricheldorf and S.-R. Lee, *Macromolecules*, **1995,** 28, 6718–6725

[12] D. E. Herbert, J. B. Gilroy, W. Y. Chan, L. Chabanne, A. Staubitz, A. J. Lough and I. Manners., *J. Am. Chem. Soc*., **2009,** 131, 14958-14968.

[13] M. Kumar, A. J. Metta-Magana, H. K. Sharma, K. H. Pannell, *Dalton Trans.* **2010,** 39, 7125.

[14] H. Berke, R. Hoffmann, *J. Am. Chem. Soc.* **1978,** 100, 7224.

[15] T. S. Piper, G. Wilkinson, J. *Inorg. Nucl. Chem.* **1956,** 3, 104−124.

[16] F. Calderazzo, *Angew. Chem.*, **1977,** 16, 299.

[17] N. A. Dunham and M. C. Baird, *J. Chem. Soc., Dalton Trans.*, **1975,** 774.

[18] X. Wang, K. Cao, Y. Liu, B. Tsang, and S. Liew, *J. Am. Chem. Soc*., **2013**, 135, 3399-3402.

[19] K. Cao, B. Tsang, Y. Liu, D. Chelladural, W. P. Power, and X. Wang, *Organometallics*, **2014**, 33, 531-539.

[20] M. Green, Westlake, D. J. Westlake, *J. Chem. Soc. A* **1971,** 367.

[21] S. G. Davies, I. M. Dordorhedgecock, K. H. Sutton, M. Whittaker, *J. Am. Chem. Soc.* **1987,** 109, 5711.

[22] K. H. Pannell and J. R. Rice, J. Organomet. Chem., **1988,** 341, 415–419.

[23] K. H. Pannell and H. K. Sharma, Organometallics, **2010,** 29, 4741–4745.

[24] O. G. Adeyemi and N. J. Coville, Organometallics, **2003,** 22, 2284–2290.

[25] J. Liu, K. Cao, B. Nayyar, X. Tian, and X. Wang, *Polym. Chem.*, **2014**, 5, 6702–6709.

[26] K. L. McFarlane, P. C. Ford, *Organometallics* **1998,** 17, 1166.

[27] H. Jiang, D. Geng, D. Liu, N. Lanigan, and X. Wang, *Chem. Eur. J.* **2017,** 23, 8280-8285.

[28] J. Liu, Z. Guan, X. Tian, J. Lin, X. Wang, *Polym. Chem*. **2016,** 7, 4419– 4426.

[29] H. Wang, L. Zhang, B. Liu, B. Han, Z. Duan, C. Qi, D. W. Park and I. Kim, *Macromol. Rapid Commun.*, **2015,** 36, 1646–1650.

[30] K. Cao, L. Peng, A. Feng, D. Liu, A. Worku, S. Liu, J. Lin, J. Yuan, X. Wang, *Chem. Eur. J.* **2018,** 24, 15380 – 15386

[31] A. Leung, J. Kang, Y. Cai, W. Chang, K. Liu, H. Xia, and X. Wang, *Organometallics* **2020,** 39, 2991−2997.

[32] T. Josse, J. De Winter, P. Gerbaux, and O. Coulembier, *Angew. Chem., Int. Ed.* **2016,** 55, 13944-13958.

[33] K. Cao, N. Murshid, L. Li, A. Lopez, K. C. Tam, and X. Wang, *Macromolecules* **2015**, 48,

7968−7977.

[34] R. B. King, *J. Am. Chem. Soc.* **1963,** 85 (13), 1918−1922.

[35] M. L. H. Green, C. R. Hurley, *J. Organomet. Chem.* **1967,** 10 (1), 188−190.

[36] Z. Gaun, D. Liu, J. Lin, and X. Wang**,** *Soft Matter*, **2017,** 13, 5130-5136.

[37] C. Kulkarni, K. K. Bejagam, S. P. Senanayak, K. S. Narayan, S. Balasubramanian, S. J. George, *J. Am. Chem. Soc* **2015,** 137, 3924-3932.

[38] S. S. Jang, T. Çağin, W. A. Goddard, *J. Chem. Phys.* **2003,** 119, 1843-1854.

[39] Abdelhamid. B. Abdelhamid, B. Ulrich M and Mustapha, *Polym. Int*. **2000**, 49, 175–183.

[40] J. Kang, J. Zhu, J. Lin, C. Han, K. Liu, and X. Wang, *Macromolecules* **2021,** 54, 7441-7447.

[41] Shortt, A. B.; Durham, L. J.; Mosher, H. S. *J. Org. Chem.* **1983**, 48 (18), 3125-3126.

[42] J. K. Stille, C. Smith, O. P. Anderson, M. M. Miller, *Organometallics* **1989,** 8, 1040–1047.

Appendix

A1 NMR characterization of FpC_{18}, $^{Cl}FpC_{18}$, $^{P}FpC_{18}$, and $P(^{P}FpC_{18})_n$

FpC_{18}, $^{Cl}FpC_{18}$, $^{P}FpC_{18}$, and $P(^{P}FpC_{18})_n$ were also characterized in the same manner as discussed in section 3.1 and 3.2.4.

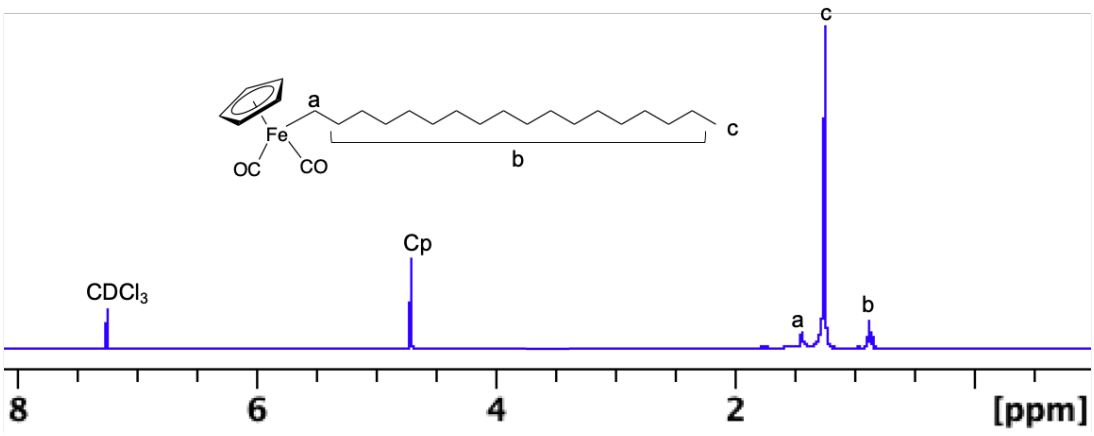

Figure A1. ^{1}H NMR ($CDCl_3$) spectrum of FpC_{18}

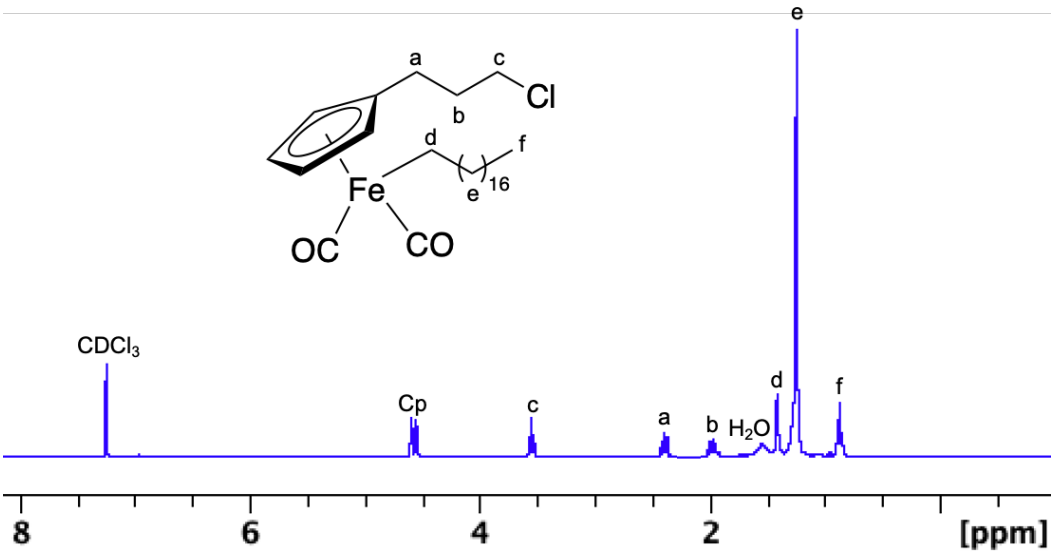

Figure A2. ^{1}H NMR ($CDCl_3$) spectrum of $^{Cl}FpC_{18}$

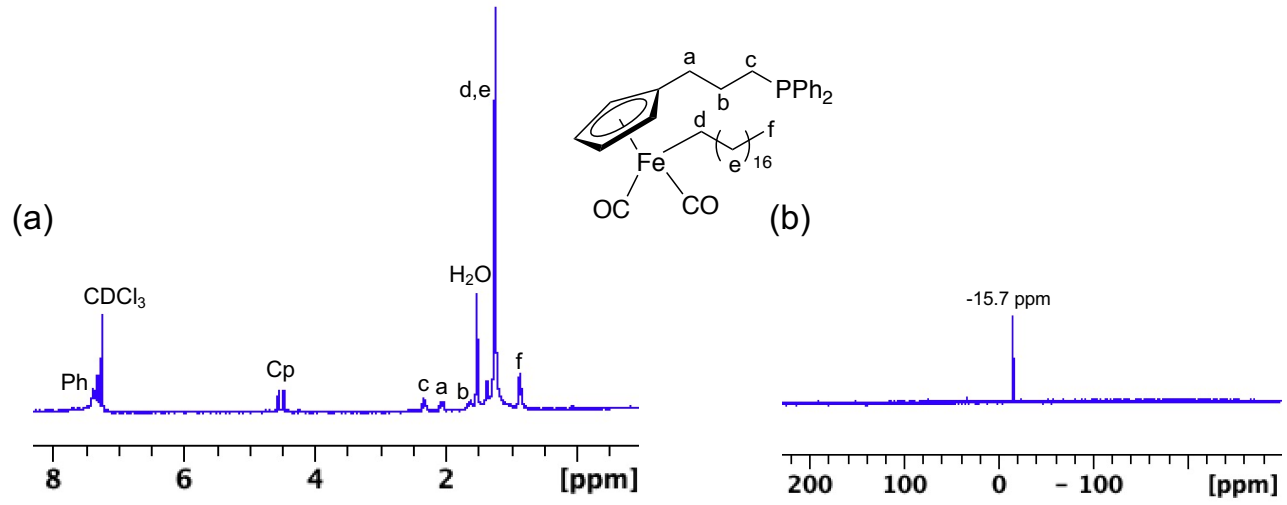

Figure A3. (a) ^{1}H NMR and (b) ^{31}P NMR ($CDCl_3$) spectra of $^{P}FpC_{18}$

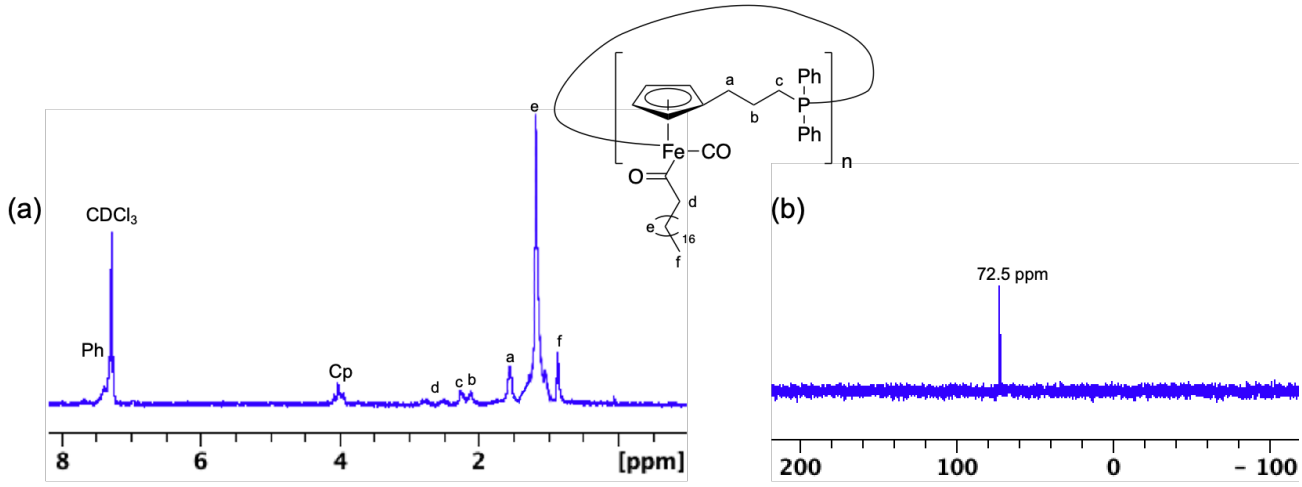

Figure A4. (a) ^{1}H NMR and (b) ^{31}P NMR ($CDCl_3$) spectra of $P(^{P}FpC_{18})_n$